



UNIVERSITAT DE
BARCELONA

Development and optimization of a Low Temperature Co-fired Ceramic suspension for Mask-Image-Projection-based Stereolithography

Joana Gonçalves Fernandes

ADVERTIMENT. La consulta d'aquesta tesi queda condicionada a l'acceptació de les següents condicions d'ús: La difusió d'aquesta tesi per mitjà del servei TDX (www.tdx.cat) i a través del Dipòsit Digital de la UB (diposit.ub.edu) ha estat autoritzada pels titulars dels drets de propietat intel·lectual únicament per a usos privats emmarcats en activitats d'investigació i docència. No s'autoritza la seva reproducció amb finalitats de lucre ni la seva difusió i posada a disposició des d'un lloc aliè al servei TDX ni al Dipòsit Digital de la UB. No s'autoritza la presentació del seu contingut en una finestra o marc aliè a TDX o al Dipòsit Digital de la UB (framing). Aquesta reserva de drets afecta tant al resum de presentació de la tesi com als seus continguts. En la utilització o cita de parts de la tesi és obligat indicar el nom de la persona autora.

ADVERTENCIA. La consulta de esta tesis queda condicionada a la aceptación de las siguientes condiciones de uso: La difusión de esta tesis por medio del servicio TDR (www.tdx.cat) y a través del Repositorio Digital de la UB (diposit.ub.edu) ha sido autorizada por los titulares de los derechos de propiedad intelectual únicamente para usos privados enmarcados en actividades de investigación y docencia. No se autoriza su reproducción con finalidades de lucro ni su difusión y puesta a disposición desde un sitio ajeno al servicio TDR o al Repositorio Digital de la UB. No se autoriza la presentación de su contenido en una ventana o marco ajeno a TDR o al Repositorio Digital de la UB (framing). Esta reserva de derechos afecta tanto al resumen de presentación de la tesis como a sus contenidos. En la utilización o cita de partes de la tesis es obligado indicar el nombre de la persona autora.

WARNING. On having consulted this thesis you're accepting the following use conditions: Spreading this thesis by the TDX (www.tdx.cat) service and by the UB Digital Repository (diposit.ub.edu) has been authorized by the titular of the intellectual property rights only for private uses placed in investigation and teaching activities. Reproduction with lucrative aims is not authorized nor its spreading and availability from a site foreign to the TDX service or to the UB Digital Repository. Introducing its content in a window or frame foreign to the TDX service or to the UB Digital Repository is not authorized (framing). Those rights affect to the presentation summary of the thesis as well as to its contents. In the using or citation of parts of the thesis it's obliged to indicate the name of the author.

ANALYSIS AND OPTIMIZATION OF DEBINDING AND SINTERING PROCESSES

CHAPTER V

The optimization of the debinding process is presented in this chapter regarding both temperature rate and atmosphere applied during this process. For this optimization, dilatometry measurement, differential scanning calorimetry and thermogravimetric analysis is presented. Moreover, the final demonstrator of the development technology is shown as a final result of the whole research developed in this work.

5.1 Introduction

Ceramic powders are inherently difficult to handle and shape into desired geometry, therefore some organic additives (dispersants, binders, plasticizers) are often required to enhance their forming capabilities. Such additives must be removed completely prior to the pieces densification at elevated temperatures – sintering process. This previous step is known as binder removal or debinding, which is the focus of this chapter.

Several strategies have been proposed for the debinding of ceramic components including thermal debinding, wicking and solvent extraction. However, the thermal debinding remains the most widely utilized process and the one used in this work.

The printed green pieces are formed by the ceramic particles and the cured resin, which bind the ceramic particle together giving strength to the green body. As said in the introduction chapter, this step is the most critical one, where the possibility of cracks and delamination formation is significantly high. Note that delamination means defects in horizontal direction, perpendicular to the printing direction. After this process, the sintering is performed nevertheless the emphasis of this chapter is the debinding once that represents the most challenging step of whole process. In fact, the debinding process is the most critical and time-consuming step during the manufacturing process.

5.5.1. Thermal debinding

Polymers are often classified into two main groups: thermoplastic or thermosetting resins. Thermoplastics are linear polymers with secondary (weak) bonding between side groups, in contrast, thermosets are covalently bonded forming a three-dimensional network. During the thermal debinding, the thermoplastics become molten or fluid with temperature and the thermosets do not flow when heated, they are decomposing directly. In this sense, the mainly defect founded in the debinding of thermosetting resins are cracks formation instead of the typical bubbles and blisters arising with thermoplastics. With thermosets, evaporation of volatile components does not involve binder redistribution by capillary forces and microcracks are formed.[1]

Nevertheless, in almost every case the polymers thermal debinding results in both volatile and solid residues (carbonaceous chars) as products of the reaction. The elimination of this carbon residue needs the presence of an oxidizing atmosphere, forming also volatile products. The produced volatile products must diffuse from the reaction site to outside of the piece, through a porous network of ceramic particles. In this regard, a small amount of polymer can produce an enormous volume of gas, which could create pressure and, consequently, internal stress on the green body is created.[2]

The polymer degradation is achieved by thermal and/or oxidative mechanisms depending on the debinding atmosphere, undergo a variety of intrinsic degradation processes, including depolymerization, random scission, and side group elimination, producing volatile degradation products, and by side reactions (cyclization and cross-linking) which form involatile carbon residue.[3] In the case of carbonaceous chars' formation, as the char layer increase, the heat flux to the virgin material decreases, reducing the decomposition rate.[4] The polymer degradation can be affected by difference factors including, polymer chemistry and structure, polymer loading, chemical interactions at polymer-ceramic interfaces, heat/mass transport, component geometry, firing atmosphere, and heating cycle.[3]

The carbon content after thermal debinding was reported to be dependent on the following parameters: the degradation behavior of the polymer, interaction of polymer with the powder particles, chemistry of the powder surface and the thermal debinding atmosphere.[5]

Regarding the polymeric load, the green bodies obtained by manufacturing methods which use low levels of binder (<10 vol%), such as pressing technology, have enough open porosity to allow volatile materials to escape from the interior to the pieces surface during the debinding step. In contrast, forming methods such as tape casting, injection molding and vat-photopolymerization processes produce green bodies that contain much higher binder loadings (15–60 vol%). Such bodies are mentioned as closed-pore compacts once their void space is nearly or completely filled with polymeric matrix. Thus, there is an initial absence of connected pore space, in other works, there no free path for the volatiles species to escape.

In this regard, this fact is the primary reason why successful debinding of these green bodies with high amount of polymeric matrix is so problematic. [3]

As said, the thermal decomposition of polymers may proceed by oxidative processes or simply by the action of heat. In many polymers, the thermal decomposition processes are accelerated by oxidants, such as air or oxygen. In these cases, the minimum decomposition temperatures are lower in the presence an oxidizing atmosphere.[4] Thus, successful debinding of ceramic green bodies clearly requires a delicate balance between the generation rate of volatile species, their elimination rates and the minimization of its gradients concentration along the green body.

In fact, to successfully remove the polymer without forming defects an extremely slow thermal debinding cycles (extending from hours to days) is required.[5] For example, a $0.17\text{ }^{\circ}\text{C}\cdot\text{min}^{-1}$ temperature rate was applied to successfully debinding a turbine rotor (maximum 75mm blade tip was $< 1\text{ mm}$) of silicon nitride, in nitrogen atmosphere.[6] Another example is the debinding of a alumina-based cylinder of 5.8 mm diameter and 25 mm length at a temperature rate of $0.05\text{-}0.2\text{ }^{\circ}\text{C}\cdot\text{min}^{-1}$. [7] Moreover, the use of non-oxidizing atmosphere is one strategy to eliminate the disruptive exothermic reactions of polymer with oxygen. Thus, inert atmosphere is usually employed to achieve degradation of higher molecular weight binder components. [6],[7] In this way, the thermal degradation proceeds uniformly throughout the volume of the polymer matrix. The degradation products diffuse towards the surface of the body. The presence of oxygen in the air atmosphere during thermal debinding induce oxidative degradation of the polymeric at the body surface and its propagation into the interior is restricted by diffusion of oxygen onto the binder, as well as by diffusion of the degradation products towards the surface and by their evaporation. [8]

Regarding vat-photopolymerization process, it was demonstrated that the cracks in the pieces might be a result of the decomposition of the photoinitiator during the thermal debinding, which release free radicals that polymerize the residual uncured monomer. Consequently, the polymerization shrinkage could cause mechanical stress resulting in cracks in the component.[6], [9]

One possibility to minimize the cracks formation during the debinding process, is the addition of non-reactive components into the photocurable suspension, such as waxes. These components degradant at lower temperatures, introducing an open structure during the debinding process, leading to an increase of the oxygen diffusion and decomposition products throughout the green object. This could in turn facilitate a smoother removal of decomposition products. Moreover, the non-reactive component was found to decrease polymerization shrinkage, leading to reduced built-in stresses in the parts.[9]

Regarding the printing parameters, it was demonstrated a relation-ship between layer thickness and cure depth. For a layer thickness of 25 μm , a cure depth of 50 μm resulted in severe delamination, whereas 150 μm gave noticeably fewer cracks on the surface, in this sense the relationship should be the cured depth 6 times higher than the layer thickness. [9], [10]

Such as in the injection molding technology, it was demonstrated that for vat-photopolymerization process the increase of “surface to volume ratio” contributes to a successful debinding. This means that thin and porous components are easier to de-bind than bulky samples. Moreover, it could be shown that a small powder diameter ($d_{50} < 1\mu\text{m}$) significantly increases the risk of intralaminar cracks during the debinding process. This could be due to the limited diffusion of the burn-off gases through the micrometer sized pores which traps the escaping gasses inside voluminous structures. [11]

Debinding cycle times of 80 - 100 hours are common for green body with smaller particles. For other ceramics like tricalcium phosphate or some bioactive glasses, larger particles can be processed (d_{50} in the range of 1 μm to 20 μm), such the LTCC used in this work. Neglecting the challenging of dispersion and stabilization of the ceramic suspension, these bigger particles allow a much easier debinding process. A debinding time of 28 hours was demonstrated for solid tricalcium phosphate structures like cylinders up to 20 mm diameter and 20 mm height. On the other hand, for bioactive glass structures, a 20 hour debinding cycle was sufficient for porous structures like trabecular bone scaffolds, heated up to 400°C. Thus, 0.2-0.3 °C/min rate are used for the debinding this debinding process.[11]

Nevertheless, for complex alumina green bodies debinding regime reported by Lithoz needs about 6-7 days depending on the realizable cooling rate.[12]

The following points describe the factors that could affect the cracks during the debinding process.

Composition of the suspensions: Defects can also be avoided by introducing open spaces into the structure by adding components or solvents designed to evaporate or decompose at a lower temperature than the thermal decomposition temperature of the polymer matrix [13][9]

Printing strategies: Residual unpolymerized monomer in the green object caused cracks during debinding, possibly owing to internal stresses caused by thermally-initiated polymerization during the debinding, thus the printing condition might be optimized.[6] Moreover, the stresses generated during the printing due to the shrinkage of the resin causes also internal stresses in the green body. For example, in the bottom-up configuration, during the detaching process of the printed layer from the vat bottom, mechanical stress is induced into the printed structure. This stress increases with the size of the contact area, i.e., for thicker walls there are a significant higher adherence on the vat bottom. This mechanical stress happens for every layer due to the process itself, which could cause delamination during debinding process. [12] [9]

Dimensions of the printed part: The mass transport becomes increasingly diffusion-limited as the features of the component increase in size, leading to long debinding times. One proposed solution to reduce delamination during debinding is by adding a plasticizing agent (non-reactive component) to reduce internal stresses generated in the part owing to polymerization shrinkage.[14]

Temperature rates: If the debinding rate is too high, volatile products from the decomposition will not have time to diffuse out from the structure, leading to pressure buildup and the formation of cracks or layer delamination [15]

Debinding atmosphere: a strategy to achieve the degradation of higher molecular weight binder components is by using an inert atmosphere. In this case, the thermal degradation proceeds uniformly throughout the volume of the polymer phase.[8],[7]

5.5.2. Liquid-phase sintering

The LTCC materials are composed by two phases, the crystalline ceramic phase and a softening point glass phase. In the used LTCC powder, the crystalline phase corresponds to the alumina particle and the glass phase to the SiO₂ based-particles. In this kind of materials, the sintering process is by Liquid-Phase Sintering (LPS). This process is possible by the incorporation of additives called wetting agents, such as SiO₂ based-powders, into the ceramic one to aid densification at lower temperature. As said previously, this enable the co-sintering with metals such as Ag of multi-materials pieces. [16]

This acceleration of densification occurs due to a "wetting" action (viscous flow mechanism) of the crystalline particles by this liquid phase. Simultaneously, the wetting agent acts as a lubricant allowing the reorientation of the particles into a more compact and dense structure. Combining these two factors, the liquid-phase additive can stimulate early densification and hence reduce required sintering temperatures by several hundred degrees. [16]

The densification of this powders has been described by three stage in liquid-phase sintering by (1) particle rearrangement, (2) dissolution and precipitation and (3) solid state sintering. The main phase of the LTCC is the crystalline phase which makes a significant contribution to the dielectric properties, however the glass phase lowers relative permittivity and increases the dielectric loss. Thus, in some cases the role of the glass phase is not only to serve as a bonding agent to hold the ceramic particles but is also to react with filler ceramic at the sintering temperature to form high quality crystalline phases. In this type of reactive system, the microstructure, phases and final properties are controlled by the sintering conditions, such as heating rate and sintering temperature. [17][16]

It should be noted that any densification or crystallization of the powder at lower temperatures, such as below 800 °C, is undesirable as this can prevent the removal of the organics and solvents causing residual carbon traces in the microstructure. Any residual carbon that may form during binder decomposition and would remain in LTCC pieces, it would adversely affect the dielectric properties on.[17]

5.2 Thermal analysis of LTCC suspensions

A characterization of the cured and uncured of both optimized LTCC suspensions and the SPOT LV resin were performed by Differential Scanning Calorimetry (DSC) and Thermogravimetric analysis (TGA) to better understand and optimize the thermal treatments, specially of the critical process of debinding.

These characterizations give important information of both weight loss and involved energy during the thermal treatment, debinding and sintering process. This study pretends to analyse the thermal degradation of the cured and uncured resin and LTCC suspension, under different condition. To this to happen, the following points will be discussed:

- 1) Cured and uncured optimized LTCC suspension were studied by DSC and TGA at different temperature rates in air atmosphere, showing differences in terms of the resin degradation during the thermal treatment. It is known that the printing process causes differences in the polymerization degree of the resin. In this sense, these two cases, cured and uncured, represents the extreme situations of the polymerization degree within the green body.
- 2) For a deeper understanding of the resin degradation depending on its polymerization degree, a TGA analysis were performed at samples with different degree of polymerization.
- 3) The uncured SPOT LV resin, which represents the extreme cases of no polymerization degree, were deeper analyzed by DSC and TGA at different temperature rates and different atmospheres, air and nitrogen (N₂).

The following study is focus on the cured and uncured LTCC suspensions, optimized at 67 wt.% of LTCC and 33 wt.% of SPOT LV resin. The TGA and DSC results are shown in Figure 5.1 for the cured LTCC suspensions with the visible light projector, representing the weight loss and the energy involved during the thermal treatment, at a constant heating rate of 10 °C·min⁻¹ until 900 °C in air atmosphere.

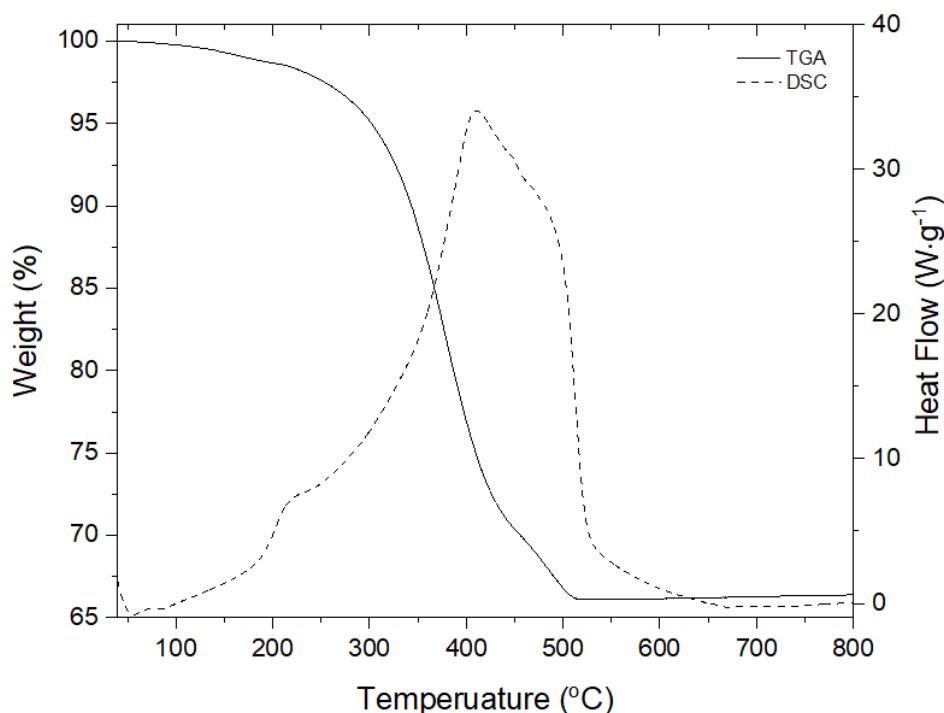


Figure 5.1 – TGA and DSC of cured LTCC suspension at $10\text{ }^{\circ}\text{C}\cdot\text{min}^{-1}$ in air atmosphere.

A total organic removal is observed, i.e., a weight loss of 33 %, below $530\text{ }^{\circ}\text{C}$. Moreover, there are three main weight loss events, associated with the formation of volatiles which must diffuse from the reaction site to outside of the piece. In this sense, the three weight loss events represent the most critical the temperature ranges during the debinding process, due to the escape of the formed gases and the possibility of cracking of the green body. The three weight loss events are described above:

- (1) the first event occurs until $200\text{ }^{\circ}\text{C}$ with a 2 wt.% of weight loss and an associated exothermic peak.
- (2) the second event is from $200\text{ }^{\circ}\text{C}$ to $430\text{ }^{\circ}\text{C}$ which corresponds to the highest rate of weight loss, removing 27 wt.% of material.
- (3) the third event is from 430 ° to $520\text{ }^{\circ}\text{C}$ removing 4 wt.% of material.

Regarding the DSC curve, it is observed two exothermic events, associated with the three weight loss events. Thus, the degradation of the resin presented in the LTCC suspensions release energy during the thermal process. Moreover, the exothermic peak with highest intensity corresponds to the last weight loss event, which could be associated with the degradation of the carbon residue formed during the polymer degradation.

The polymerization of uncured resin and/or the different photopolymerization conversion presented in the printed pieces could be the reason of the crack formation during debinding process. In this regard, a TGA and a DSC was performed to the uncured LTCC suspension, simulating the extreme case where the printed pieces present non-cured zones. Figure 5.2 shows the DSC and TGA results for a rate of $10\text{ }^{\circ}\text{C}\cdot\text{min}^{-1}$ in air atmosphere.

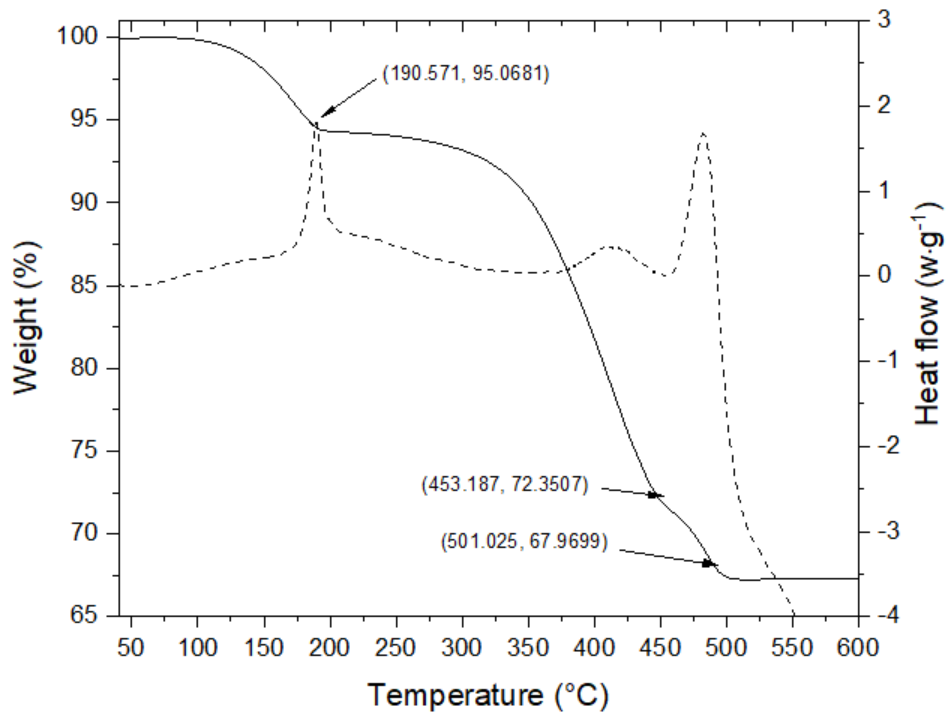


Figure 5.2 – DSC and TGA of uncured LTCC suspension at $10\text{ }^{\circ}\text{C}\cdot\text{min}^{-1}$ in air atmosphere.

It is observed a weight loss of 5 wt.% until $190\text{ }^{\circ}\text{C}$, which was not observed in the TGA of the cured suspension (Figure 5.1). Thus, this first weight loss event is related to the degradation of the monomer.

At the end of the first weight loss an exothermic event at $190\text{ }^{\circ}\text{C}$ is detected and it is related to the exothermic polymerization of acrylates resins. The photoinitiator is thermally decomposed during heating, resulting in free radicals which might cause the polymerization of the resin. Consequently, the polymerization of the resin leads to shrinkage, which may produce mechanical stresses on the green body resulting in the cracks formation on the green body. In this regard, if the polymerization of the resin was not completed during the

printing process, both volatile outflow and polymerization could be the cause of cracking of the green body until 190 °C.

After the first exothermic event, the weight lost remains almost constant for 50 °C. Finally, the decomposition of the crosslinked resin occurs between 300 to 500 °C with two associated exothermic events, which can also cause the cracking of pieces. The total weight loss during the thermal analysis is 33 %, which represents the total removal of the organic material.

The TGA of the cured and uncured LTCC suspension are significantly different, thus nonuniformities on the resin polymerization during the printing process causes different thermal decomposition. In this sense, it is important the analysis of the thermal degradation of both cured and uncured resin.

The following results are related to the resin (without ceramic particles) and the accurate analysis of its behaviors under the thermal debinding. The goal of this experiment is to evaluate if the polymerization degree of the resin changes along the layer thickness, due to the attenuation of light. Figure 5.3 shows a scheme of the studied zones of the cured resin using the visible light projector, the one used on the MIP-SLA machine. Zone 1 represents the zone of highest polymerization degree, zone 2 the less polymerization degree.

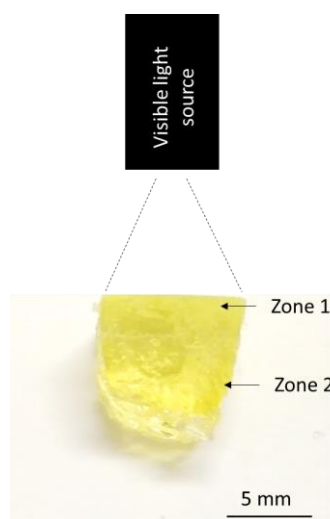


Figure 5.3 – Scheme of the cured resin along the cured depth

Figure 5.4 shows the TGA results of the different zones performed at $10\text{ }^{\circ}\text{C}\cdot\text{min}^{-1}$ in air atmosphere. The TGA of the liquid resin is also presented in the graphic, representing the extreme cases of totally uncured resin (liquid) and the maximum of curing using a UV source (UV cured)

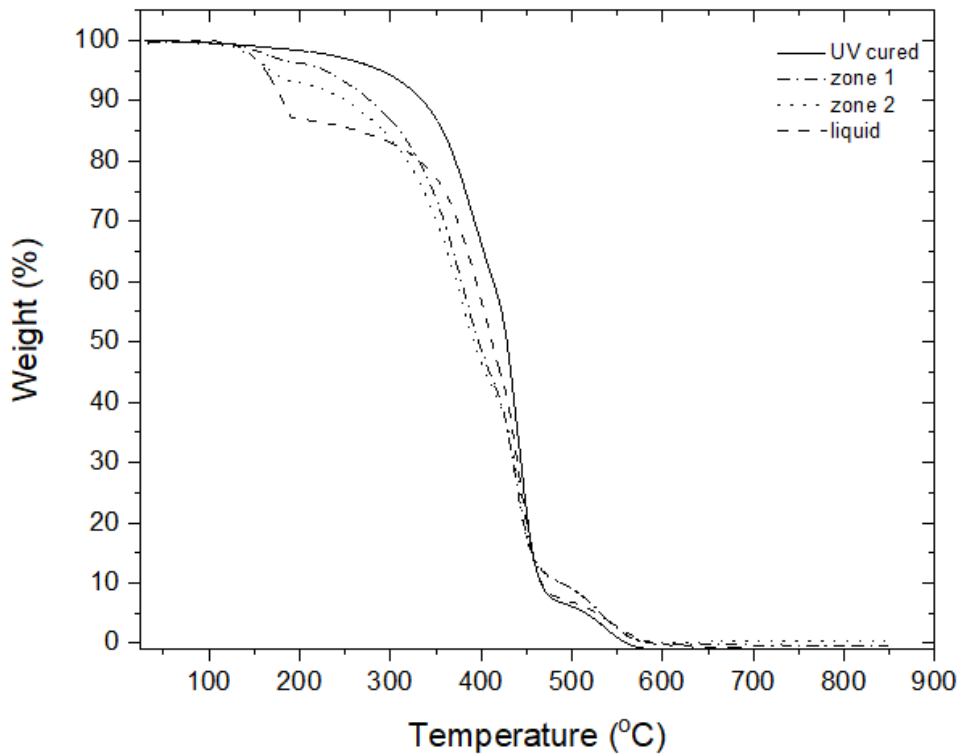


Figure 5.4 -TGA of different polymerization degree of the resin at $10\text{ }^{\circ}\text{C}\cdot\text{min}^{-1}$ in air atmosphere

The main differences between all results are observed until $350\text{ }^{\circ}\text{C}$. A weight loss starts at $120\text{ }^{\circ}\text{C}$ for the samples from zone 2 and zone 3. This weight loss event is not observed for zone 1 and becomes higher as the degree of polymerization decreases. Note that the extreme case of the liquid resin, which is not polymerized, the weight loss is greater than in the other cases. Thus, this weight loss is associated to the degree of polymerization.

As said previously, after the weight loss an exothermic peak is presented for the uncured resin which are associated with the polymerization of the monomer. However, the weight loss event between $450\text{--}600\text{ }^{\circ}\text{C}$ has the same behavior for all samples, which means that the polymer formed during the thermal treatment has the same decomposition behavior as the

one which was totally cured by the light source (zone 1). Moreover, the rates of weight loss after the first weight loss event, have similar behavior.

This analysis confirms that the thermal degradation of the polymer will occur differently depending of the polymerization degree. In fact, the differences of the polymerization degree along the layer thickness is a reality during the printing process, due to the attenuation of the light. In this regard, the different thermal degradation behavior must be considered for the optimization of the debinding process.

It is known that the used non-oxidative atmosphere during the debinding process could improve the cracking of the green body. In this regard, the TGA analysis was also performed in nitrogen atmosphere. Figure 5.5 shows the TGA results of the cured resin (zone 1) performed in both air and N_2 atmosphere at a temperature rate of $10\text{ }^\circ\text{C}\cdot\text{min}^{-1}$ and $0.3\text{ }^\circ\text{C}\cdot\text{min}^{-1}$.

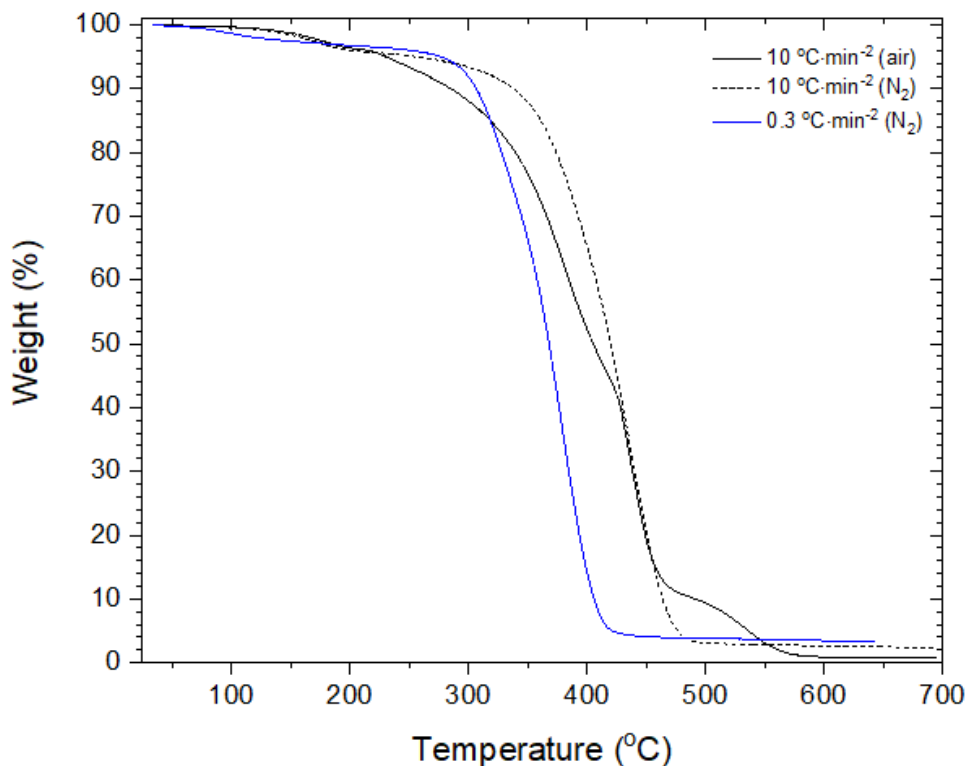


Figure 5.5 – TGA of cured resin performed at $10\text{ }^\circ\text{C}\cdot\text{min}^{-1}$ in air and N_2 atmosphere and $0.3\text{ }^\circ\text{C}\cdot\text{min}^{-1}$ in N_2 .

As said in the analysis of the TGA of the cured LTCC suspension (Figure 5.1), the highest weight loss event occurs at 385 °C for the experiment performed in air atmosphere. This result is also observed for the resin itself, as seen in Figure 5.5. However, using a N₂ atmosphere the weight loss event occurs for higher temperature. Moreover, the first weight loss event is observed in all curves, associated with the degradation of the residual monomer. This event occurs independently of the atmosphere and the temperature rate, however with different behavior which will be discussed later.

Additionally, the third weight loss event observed in the air atmosphere experiment is not observed in the case of N₂ atmosphere one. Both volatile and solid residues (carbon chars) are formed during the thermal debinding. However, the elimination of the carbon residue needs the presence of an oxidizing atmosphere. In this regard, the final weight loss observed in air atmosphere experiment is associated to the elimination of the carbon residues, which does not occur in N₂ atmosphere. It is observed a total removal of organic part for the experiment in air atmosphere, and a 99 % in the N₂ case. The incomplete elimination of the organic part is associated to the carbon residue which cannot be eliminated due to the absence of oxygen in this experiment.

In this sense, the main differences in terms of thermal degradation are observed in the degree of polymerization of the resin, i.e., the exothermic peak and the weight loss between 120 to 190 °C depending of the degree of polymerization.

Thus, the following results are just focus on the first weight loss and exothermic peak, once the thermal degradation for higher temperatures are similar for both uncured and cured resin.

This study was performed with uncured resin, representing the extreme case of inhomogeneities of polymerization during the printing process. Different temperature rates at air and N₂ atmospheres were studied for a deeper understanding of the exothermic peak and the weight loss until 190 °C. This study will be further related with the debinding optimization, where the temperature rate, used atmosphere and printing parameters of the green bodies are the main factors that affect the debinding process.

The results for a temperature rate of 0.3 and 10 °C·min⁻¹ in air atmosphere are displayed in Figure 5.6. The DSC curves are presented in a shorter temperature range for a better visualization of the exothermic peaks.

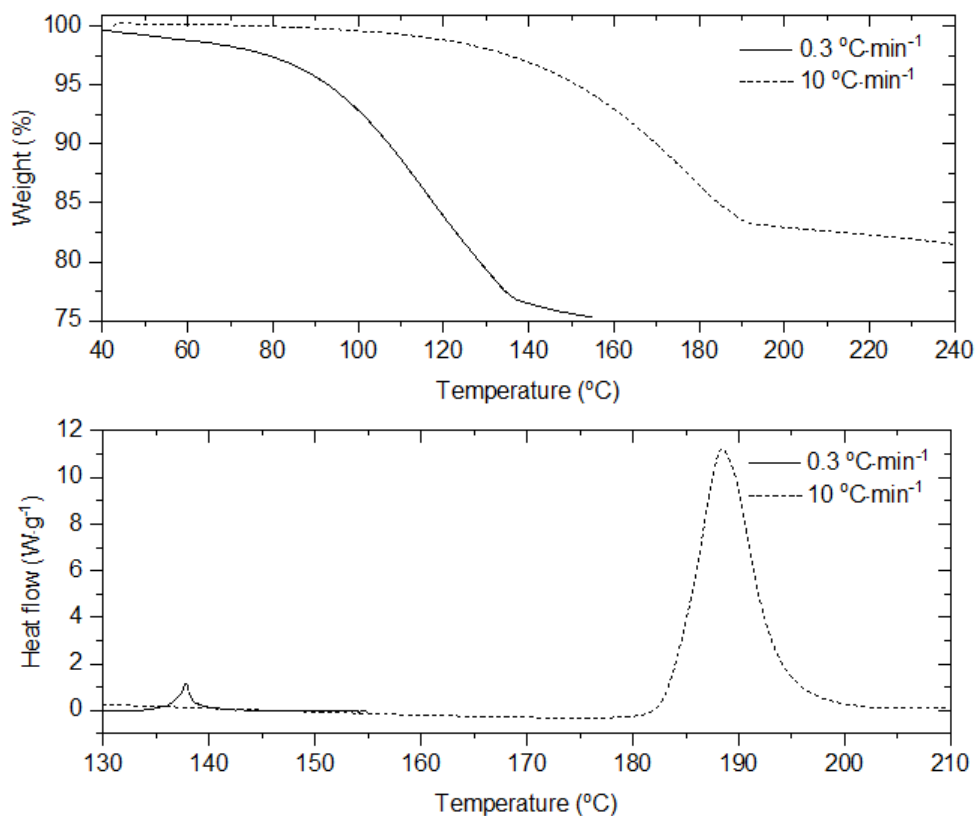


Figure 5.6 – TGA and DSC at different rates: 0.3 and 10 °C·min⁻¹ in air atmosphere of the uncured resin.

In both cases, the exothermic event occurs at the end of the weight loss, nevertheless for lower temperature rates the exothermic peak has less intensity. After the DSC/TGA thermal analysis the resin was cured in both cases, proving the association between the exothermic event and the polymerization of the resin.

Apart from the exothermic event, a weight loss is observed in both cases, resulting in a 17 wt.% for the 10 °C·min⁻¹ and 23 wt.% for 0.3 °C·min⁻¹. As said previously, this weight loss is associated to the monomer decomposition. After the exothermic peak, the TGA curve change its slope which means a decrease of the weight loss rate. This weight loss rate

variation is clearer in the case of the $10\text{ }^{\circ}\text{C}\cdot\text{min}^{-1}$, and it is related to the degree of polymerization of the resin, which occurs during the thermal analysis.

It seems that in the case of the $0.3\text{ }^{\circ}\text{C}\cdot\text{min}^{-1}$ the degree of polymerization is less than in the case of $10\text{ }^{\circ}\text{C}\cdot\text{min}^{-1}$, thus the resultant polymer has less molecular weight. Consequently, its weight loss rate, after the exothermic peak, is higher than in the case of the $10\text{ }^{\circ}\text{C}\cdot\text{min}^{-1}$. [18]

Moreover, it is observed that the weight loss is stopped by the exothermic peak. This can be explained by the polymerization of the monomer forming a polymer with higher molecular weight. Therefore, such energy is not enough for the degrade the cross-linked polymer.

As said, the results of the debinding process could be improved, i.e., forming less defects, if the thermal treatments are performed in absence of oxygen. In this regards a TGA and DSC analysis of the uncured resin was also performed under nitrogen atmosphere.

Figure 5.7 shows the TGA and DSC results of the uncured resin, performed at a temperature rate of $10\text{ }^{\circ}\text{C}\cdot\text{min}^{-1}$ in both air and N_2 atmospheres. The DSC curves are presented in a shorter temperature range for a better visualization of the exothermic peaks.

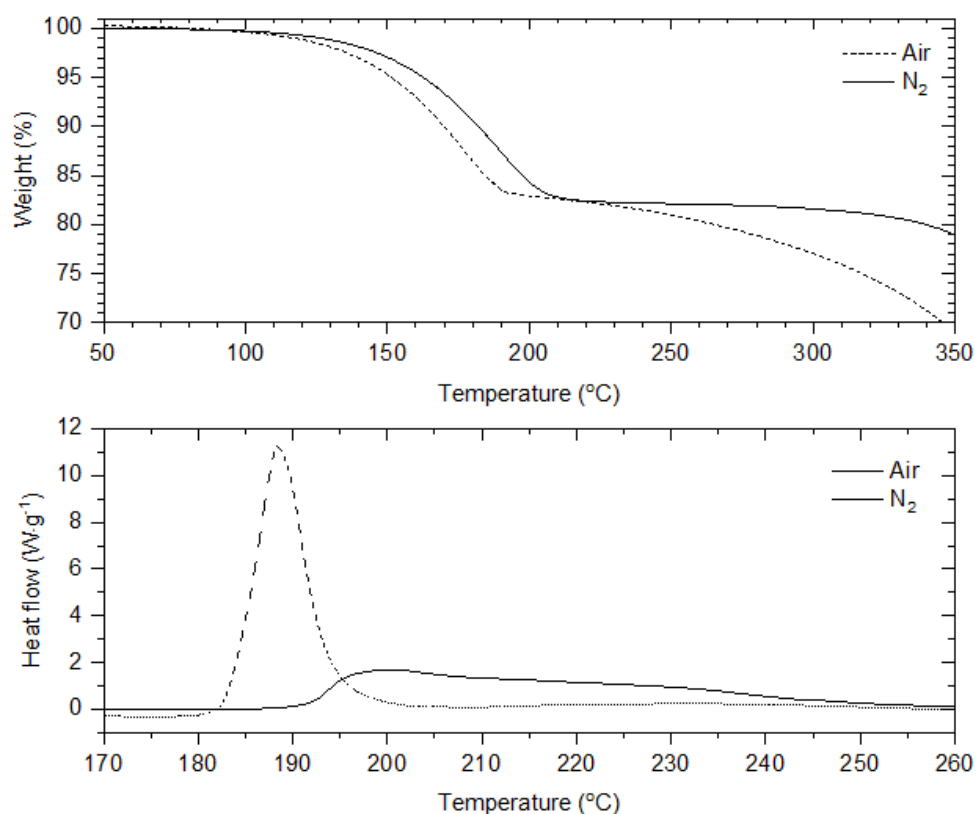


Figure 5.7 – TGA and DSC results at $10\text{ }^{\circ}\text{C}\cdot\text{min}^{-1}$ in air and N_2 atmospheres of the uncured resin.

The weight loss is almost the same for both cases, around 17 wt.%, thus the weight loss and resultant gases amount are independent of the atmosphere. However, the weight loss in N_2 after the exothermic peak remains constant during 100 °C and it is not observed in the case of the air atmosphere experiment. These results suggest that the resultant polymer presents different polymerization degree and or a different cross-linked structure, depending of the used atmosphere. Besides, the presence of a non-oxidative atmosphere significantly decreases the intensity of exothermic peak.

To analyze energy involved in the polymerization reaction the DSC of both curves was analyzed in function of the time. Figure 5.8 shows the area of both exothermic curves, which represents the specific enthalpy, of the polymerization reaction and the maximum of heat release (y_{max}).

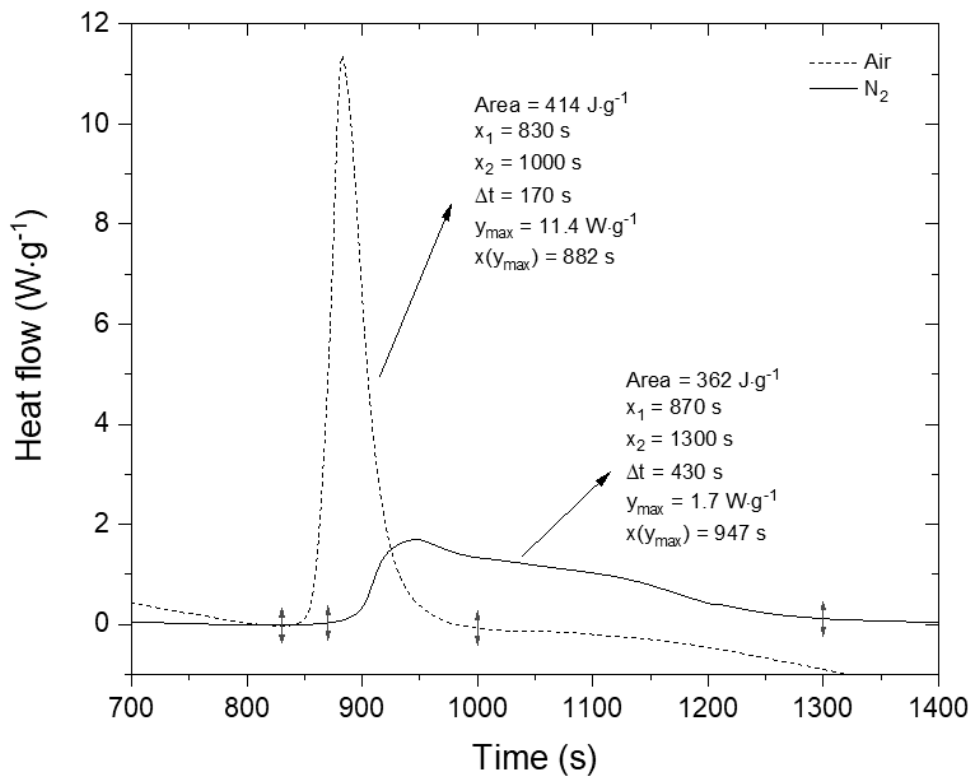


Figure 5.8 – DSC results at $10\text{ }^\circ\text{C}\cdot\text{min}^{-1}$ in air and N_2 atmospheres of the uncured resin, in function of time.

The specific enthalpy is slightly different in both cases, $414\text{ J}\cdot\text{g}^{-1}$ and $362\text{ J}\cdot\text{g}^{-1}$ for the experiment in air and in N_2 atmosphere, respectively. This means, that the energy involved in the polymerization reaction is slightly different for each atmosphere. Moreover, the maximum value of energy release is much higher in the air atmosphere experiment, $11.4\text{ W}\cdot\text{g}^{-1}$ and $1.7\text{ W}\cdot\text{g}^{-1}$ for the air and N_2 experiment, respectively. Note that in the case of the air atmosphere, the polymerization process occurs in a short range of temperature, i.e., during 170 s. On the other hand, in the N_2 experiment the energy is released during 430 s, approximately. In this regard, the energy released by the exothermic even is more gradual in the N_2 experiment than in the air one.

The exothermic peak is related with the polymerization of the uncured resin by the thermal degradation of the photo-initiator, which is dissociated into radicals. These radicals will further react with the monomer molecules, forming a radical monomer, which will react successively with the other monomer molecules (propagation step). This reaction release a

certain amount of energy, which is different depending of the atmosphere. Moreover, the energy is released for longer periods in the N₂ atmosphere, than in air atmosphere.

It is known that in acrylate systems, the presence of oxygen inhibits the polymerization process [19], illustrated in Figure 4.9.

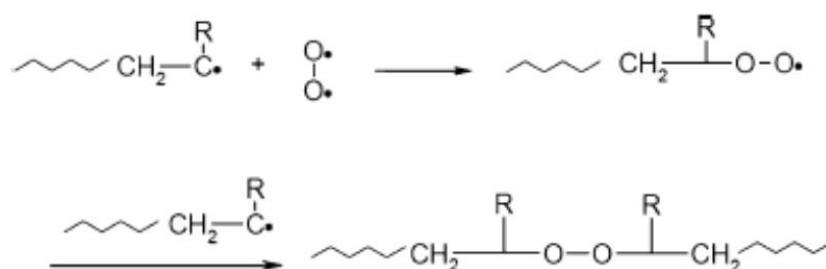


Figure 4.9 – General situation of inhibition of the polymerization process due to the oxygen. [19]

Once the photoinitiator is decomposed and reacts with the monomer, forming the radical monomer, the propagation process can be stopped by the oxygen molecules. This is explained by the attachment of the oxygen onto the reactive monomer, resulting in a molecule with an oxygen radical end, unable to initiate the polymerization. Thus, its recombination reactions with radical monomer terminate the polymerization.

In this regard, once the photoinitiator is terminally degraded both phenomena, oxidation of the reactive monomer and recombination with other reactive monomer, is presented in the experiments performed in air atmosphere. [20]

The thermal decomposition of the photoinitiator is presented in both experiments, in air and in N₂, but the mainly difference is the present of the oxygen in the air experiment. In this regard, the oxidation of the reactive monomer does not occur in the N₂ atmosphere experiment.

Therefore, the oxidation of the reactive monomer leads to an associated energy release. Note that both exothermic events occur in the air atmosphere experiment, the oxidation of the reactive monomer and the recombination of the reactive monomers. Therefore, this

could be the explanation for both observed differences, i.e., the involved energies of the exothermic peak and the weight loss after the exothermic peak.

Note that in the N_2 atmosphere experiment the weight remains constant during 100 °C, on the other hand, in the air atmosphere the weight loss decreases after the exothermic peak, with a different rate. This means that in the N_2 atmosphere experiment the formed polymer presents a higher molecular weight than the one formed in the air atmosphere.

As seen previously in the DSC results performed in air atmosphere at different rates, Figure 5.6, the energy release from exothermic event decreases for lower temperature rates. Concerning this result, a DSC and TGA was performed at $0.3\text{ °C}\cdot\text{min}^{-1}$ in N_2 atmosphere to the uncured resin. Figure 5.10 shows the comparison of the experiments performed at N_2 and air atmosphere with a temperature rate of $0.3\text{ °C}\cdot\text{min}^{-1}$.

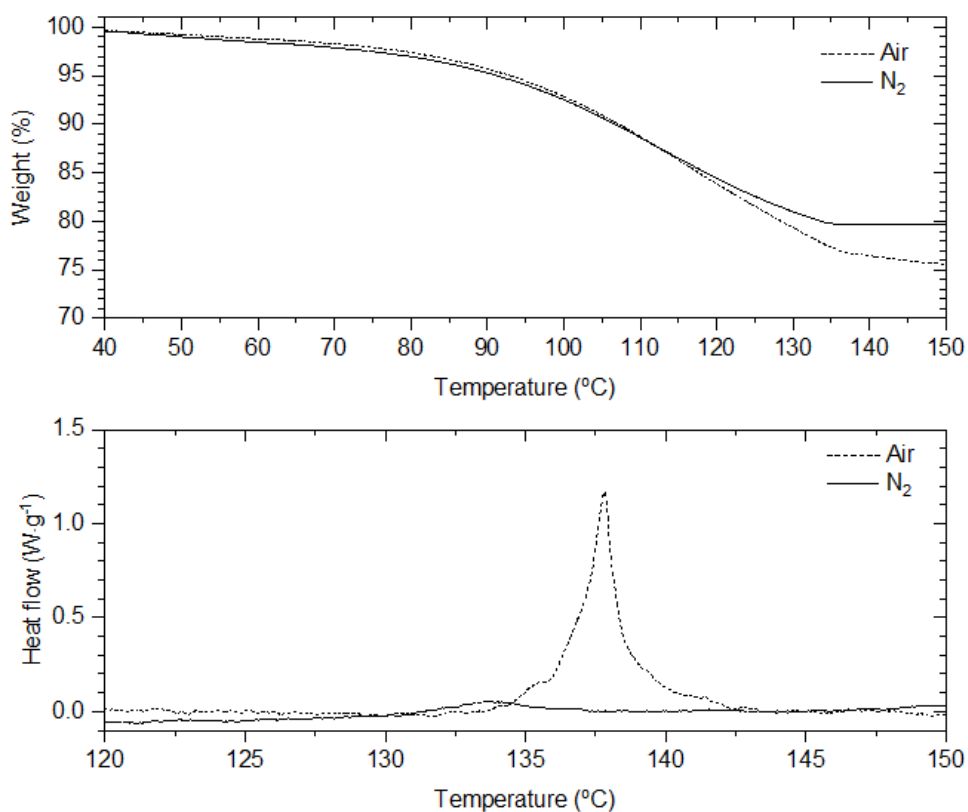


Figure 5.10 – DSC and TGA of uncured resin at $0.3\text{ °C}\cdot\text{min}^{-1}$ in air and N_2 atmosphere.

The TGA results reveal that the weight loss presents practically the same behavior for both atmospheres, with a total weight loss of 21 and 23 % for the N_2 and air atmospheres,

respectively. This means that reducing the temperature rate, this weight loss increases a 5 % (see Figure 5.7). However, in the N_2 results is observed a no weight loss after the exothermic peak where no variation of weight is observed, such as in the previous results shown in Figure 5.7.

Moreover, the intensity of the exothermic peak decreases drastically using the N_2 atmosphere. Figure 5.11 shows the DSC results in function of time for the experiments performed at $0.3\text{ }^\circ\text{C}\cdot\text{min}^{-1}$ for both atmospheres.

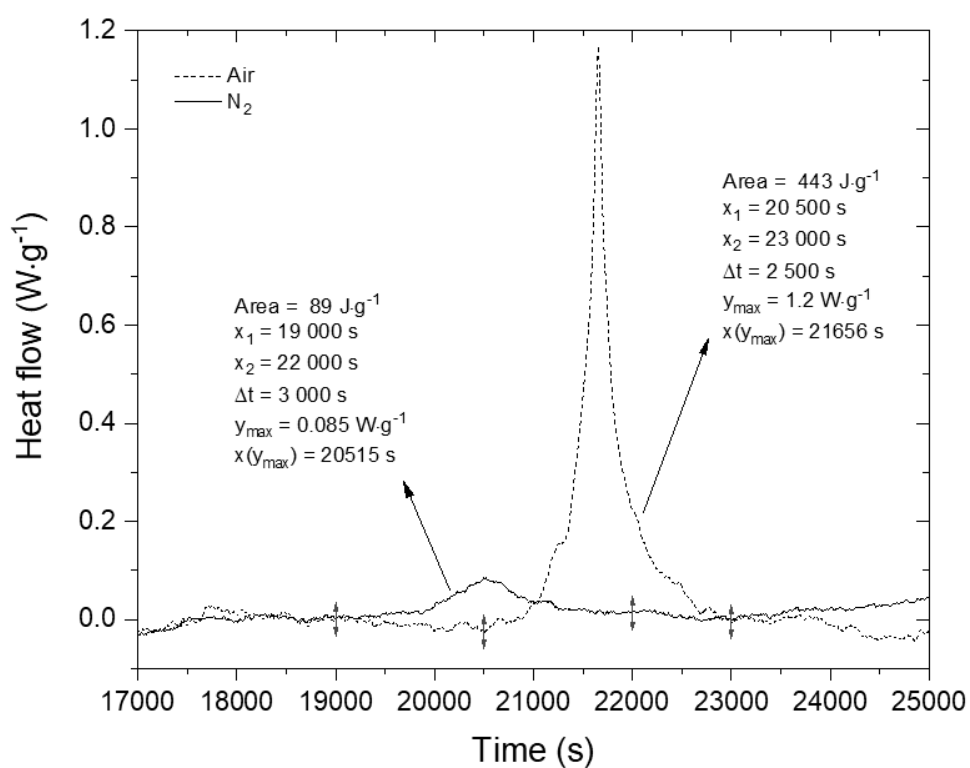


Figure 5.11 – DSC results at $0.3\text{ }^\circ\text{C}\cdot\text{min}^{-1}$ in air and N_2 atmospheres of the uncured resin, in function of time.

Furthermore, it is observed a small peak in the $0.3\text{ }^\circ\text{C}\cdot\text{min}^{-1}$ in air atmosphere which is related to the decomposition of the photo-initiator, which will promote the polymerization of the monomer.

In comparison with the experiments performed at $10\text{ }^\circ\text{C}\cdot\text{min}^{-1}$ in air, the energy release in the $0.3\text{ }^\circ\text{C}\cdot\text{min}^{-1}$ in air atmosphere is almost the same, $443\text{ J}\cdot\text{g}^{-1}$. However, this energy is releasing for 2500 seconds instead of 170 seconds (observed for the $10\text{ }^\circ\text{C}\cdot\text{min}^{-1}$

experiment). This means that reducing the temperature rate, the polymerization process occurs in a more gradual way and the maximum energy release decreases.

Additionally, the exothermic event release less energy when the thermal conditions are performed at low temperature rate and in N₂ atmosphere, with a specific enthalpy of 89 J·g⁻¹. In the last case the maximum of energy release is 0.085 W·g⁻¹, which is significantly less when compared with the one performed in air atmosphere which is 1.2 W·g⁻¹.

The differences in the specific enthalpy in both cases are greater than the ones observed in the 10 °C·min⁻¹ experiment (Figure 5.8) which becomes more evident decreasing the temperature rate. As said previously, this difference could be explained by the oxidation of the radical monomer under the presence of oxygen, releasing more energy than in absence of oxygen.

In fact, comparing the extreme cases of 10 °C·min⁻¹ in air atmosphere and 0.3 °C·min⁻¹ in N₂ atmosphere, the maximum intensity of the exothermic peak decreases drastically, from 11.4 to 0.085 W·g⁻¹. Moreover, the specific enthalpy also decreases drastically, from 414 J·g⁻¹ to 89 J·g⁻¹, 10 °C·min⁻¹ in air atmosphere and 0.3 °C·min⁻¹ in N₂ atmosphere, respectively.

In conclusion, combining both N₂ atmosphere and slow temperature rates, the maximum energy intensity of the exothermic peak is reduced. Moreover, the energy release during the polymerization process reduces also with both thermal conditions, i.e., with N₂ atmosphere and slow temperature rates. Both factors may improve the debinding process due to the inhomogeneities of the photopolymerization degree presented during the printing process.

The next section is related to the shrinkage and/or expansion of the green body during the debinding and sintering. For this analysis, a dilatometry method was used, which is a thermo-analytical method for measuring the shrinkage or expansion of materials over a controlled temperature regime.

5.3 Dilatometry of LTCC green bodies

The dilatometry measurements will be discussed in this session to evaluate the shrinkage dependence with temperature rates and printing parameters on the debinding and sintering process

The shrinkage of the green body was analyzed by an optical dilatometer from Expert System Solutions. As said, this technique was used to measure the shrinkage during the thermal treatment, i.e., debinding and sintering processes. Figure 5.12 shows the optical dilatometer, the chamber furnace with a sample and the scheme of the shrinkage analysis. The shrinkage results represent the dimensional variation in the Z-direction, which corresponds to the printing direction, allowing the visualization of the delamination defect during the thermal treatment. The preparation of the samples was performed by cutting a printed cylinder into a smaller piece around 2 x 2 x 3 mm, due the difficult to print it directly.

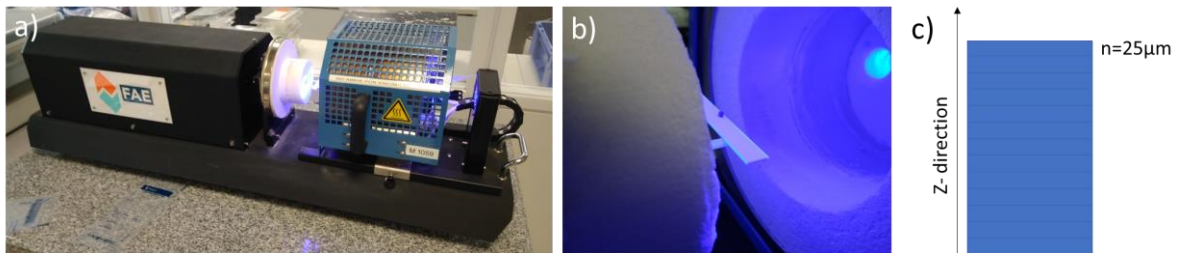


Figure 5.12 – Image of the a) horizontal optical dilatometer b) chamber with a sample of 2 x 2x 3 mm and c) scheme of the printing direction of the sample.

A study of temperature rate was initially performed to the samples printed with 25 µm of layer thickness and 10 seconds of exposure time. In order to study both, debinding and sintering processes, this study was performed until 900 °C. This study was performed at different temperature rates, once it is an important parameter during the thermal treatment to prevent the cracking of the green body.

Figure 5.13 shows the dilatometry results, i.e., the shrinkage in the z-direction during the thermal treatment until 900 °C. This study was performed at different temperature rates, to

find out its relationship between shrinkage percentages and related temperatures. The selected temperature rates were 0.1, 0.5, 1 and 10 °C·min⁻¹ in air atmosphere.

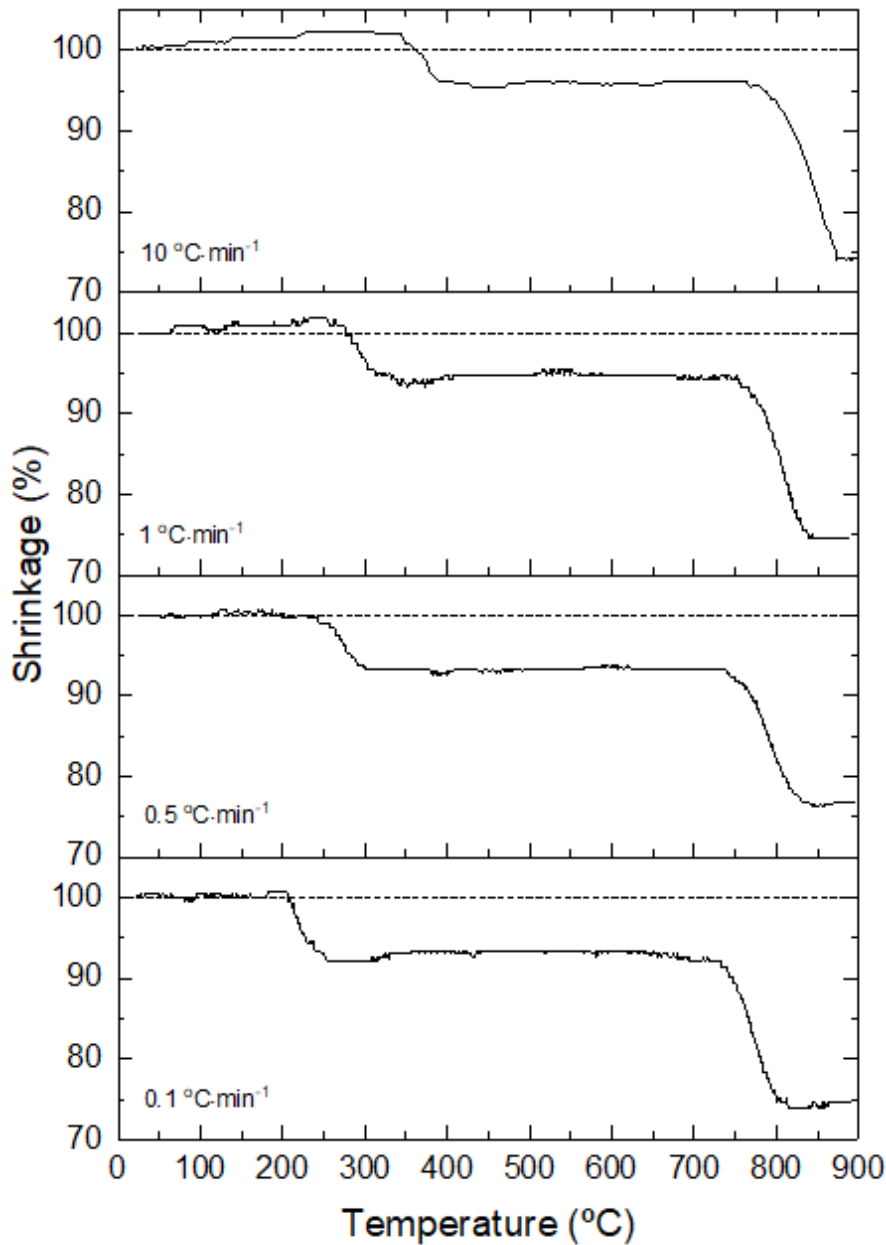


Figure 5.13 – Dilatometry results of a sample of 25 μm of layer thickness at different rates of thermal treatment in air atmosphere.

It is observed two shrinkage events in all cases, the first one corresponds to the binder removal (debinding) and the second one is related to the sintering process. As expected, the temperature of both events is dependent of the temperature rates. It is observed that the shrinkage occurs for lower temperature values as the temperature rates decrease

Moreover, an expansion of the green body for both cases, 1 and 10 °C·min⁻¹, is observed before the debinding shrinkage. In this regard, as the temperature rate increases an expansion of the green body is more evident. This expansion before the first shrinkage is not observed at lower temperatures rates, 0.5 and 0.1 °C·min⁻¹

This expansion observed in the samples for higher temperature rates is related with the thermal degradation of the resin. Figure 5.14 shows the correlation between the shrinkage and the TGA results of the cured and uncured LTCC suspension, already presented in Figure 5.1 and Figure 5.2. All results were performed at the same thermal condition, i.e., a temperature rate of 10 °C·min⁻¹ and in air atmosphere.

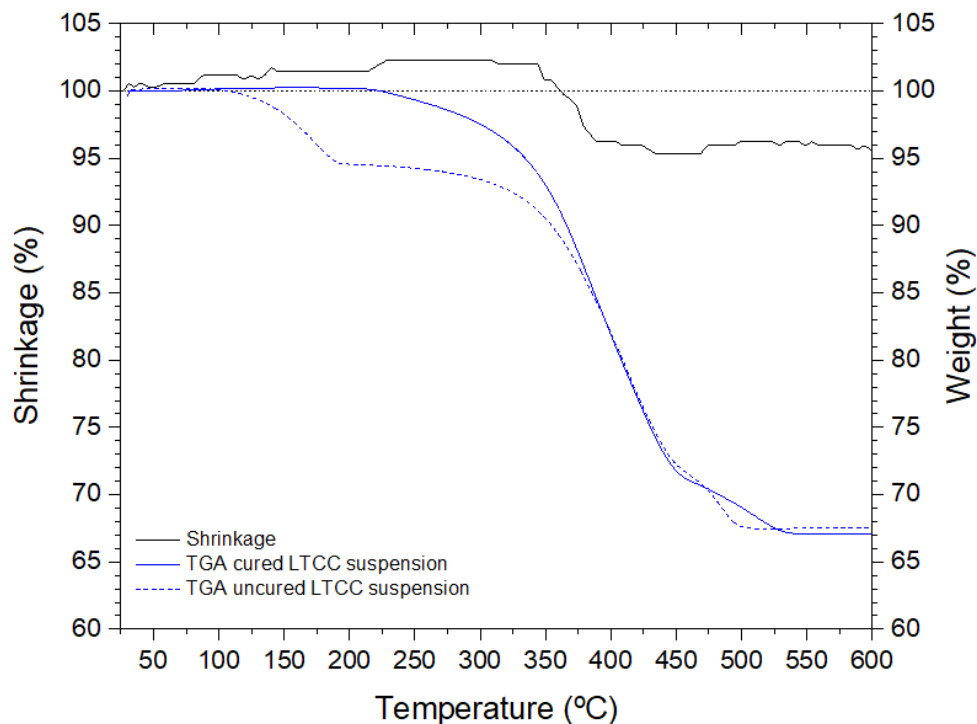


Figure 5.14 – Derivative weight loss of cured LTCC suspension and shrinkage of a printed piece performed at 10 °C·min⁻¹ in air atmosphere.

It is observed that the highest weight loss event of both cured and uncured LTCC suspension, corresponds to the shrinkage event. Note that the printed parts present a photocuring differences along the layers thickness and along the whole printed pieces. In this regard, the expansion observed in the dilatometry analysis, could be associated with the gases formed during the thermal decomposition of both extremes cured and uncured resin. Moreover,

the exothermic peak associated to the thermal polymerization of the less polymerized zones could also contribute for this thermal expansion. As seen before, as the temperature rate increases the release energy intensity of the exothermic peak increases, thus more energy per unit of time is release causing the expansion of the green body. On the other hand, for lower temperature rates, the expansion were not observed once the escape of the volatiles is performed in the gradual manner and the energy intensity of the exothermic peak is must lower.

The final shrinkage of the debinding process is almost the same in all cases, around 7.5 %, independent of the temperature rates. Table 5.1 shows the initial and final temperature of the debinding event and its associated shrinkage.

Table 5.1 – Initial and final temperature and related shrinkage of de debinding event at different temperature rates.

Debinding rate (°C/min)	Initial Temperature (°C)	Final temperature (°C)	Shrinkage (%)	Expansion (%)
0.1	205	260	8	-
0.5	220	310	7	-
1.0	260	340	8	1.7
10	345	440	7	2.2

Thus, the first shrinkage event is related to the percentage of organic material (resin) which is around 33 wt.%, resulting in a dimensional reduction of 7.5 %. The expansion observed in both 1 and 10 °C·min⁻¹ sample is 1.7 and 2.2 %, respectively. In the last two cases, the shrinkage value was calculated considering the expansion values.

As said, the second shrinkage event is related to the sintering process, occurring for different temperatures depending also the temperature rates. Table 5.2 shows the initial and final temperatures values where the shrinkage take place. The total shrinkage of the whole process is presented for all temperature rates, taking into account the expansion presented in the 1 and 10 °C·min⁻¹ cases.

Table 5.2 - Initial and final temperature and related shrinkage of the sintering event at different temperature rates.

Sintering rate (°C·min ⁻¹)	Initial Temperature (°C)	Final temperature (°C)	Sintering shrinkage (%)	Total shrinkage (%)
0.1	720	820	19	26
0.5	740	850	17	24
1.0	750	870	21	27
10	760	880	22	26

It is observed that the final shrinkage is almost the same for all cases, around 26 %, even occurring at different temperature, depending on the temperature rates.

It is observed that the initial temperature of the shrinkage event in the debinding process presents a higher dependence of the temperature rate. Note that for the 0.1 °C·min⁻¹ sample the shrinkage occurs at 205 °C, while for the 10 °C·min⁻¹ sample the shrinkage occurs for 345 °C, which means a temperature difference of 140 °C. On the other hand, the shift of the initial temperature of the sintering event is 40 °C for the extreme cases, i.e., for the 0.1 °C·min⁻¹ and the 10 °C·min⁻¹ samples.

As said previously, the relationship between the layer thickness and cure depth could be a decisive factor on the delamination of the green body. In this regard, a dilatometry study was performed at pieces printed with different layer thickness applying the same energy dose. Figure 5.15 shows the dilatometry results performed at a 1 °C·min⁻¹ until 900 °C in air atmosphere, for the samples printed with different layer thickness, 25, 50 and 75 µm and an exposure time of 10 seconds.

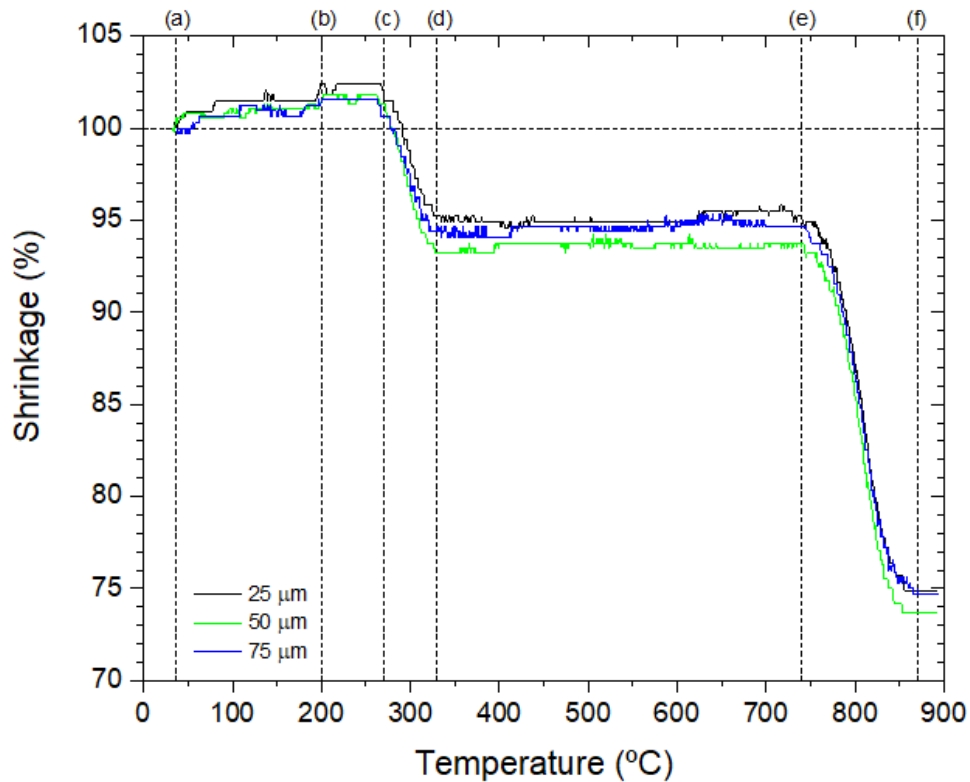


Figure 5.15 – Shrinkage in function of temperature at $1\text{ }^{\circ}\text{C}\cdot\text{min}^{-1}$ in air, for different layer printing conditions.

It is observed that both shrinkage events, debinding and sintering, occur at the same temperatures. The expansion before the debinding shrinkage is observed for all samples, which means that is independent of the printing parameter. Moreover, there is no clear relationship between the printing parameter and the shrinkage of the samples. There is a variation of 1.5 % for the debinding shrinkage and 1 % for the final shrinkage, which could be associated to the sample preparation. In this sense, the layer thickness does not affect the total shrinkage, apparently.

Figure 5.16 shows the dilatometry images of the 75 μm sample, showing the temperature, time and shrinkage at different phases. These phases are identified in Figure 5.15.

The dashed lines in Figure 5.16 serve as a guide to visually observe the expansion and shrinkage during the thermal treatment.

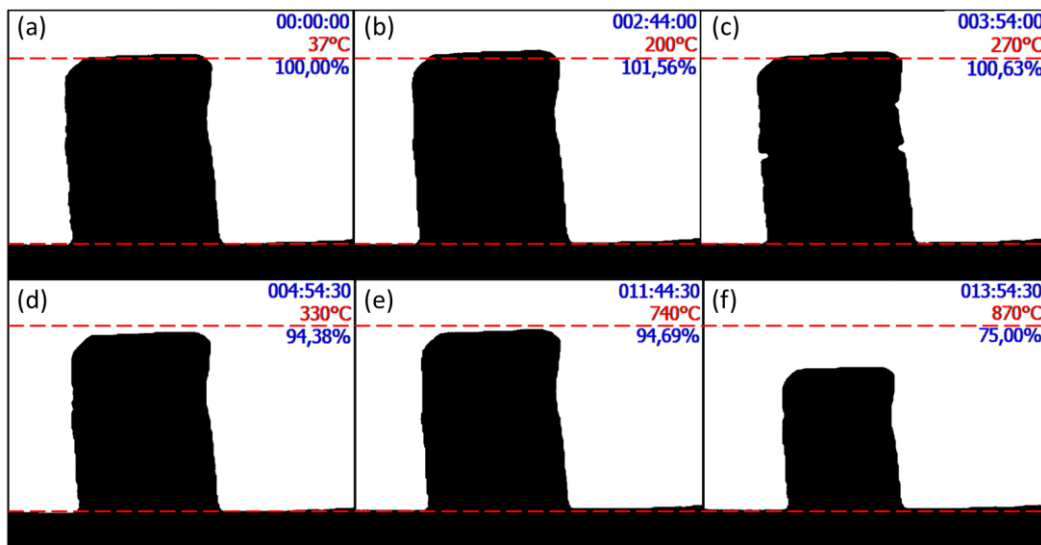


Figure 5.16 – Dilatometry images at different temperatures of the samples printed with 75 μm layer thickness, performed at $1\text{ }^{\circ}\text{C}\cdot\text{min}^{-1}$ in air atmosphere.

Although the shrinkage behavior is similar in all samples, a cracks formation was observed on the 50 and 75 μm of layer thickness samples at a temperature of 270 $^{\circ}\text{C}$, Figure 5.16 c. This temperature corresponds to final stage of the expansion and at the begging of the shrinkage.

It is known that the polymerization reaction is associated to a shrinkage, and, at the same time an energy release from the exothermic peak, as shown in the DSC analysis. Thus, if the polymerization of the resin is not uniform, some internal stress can be produced due to the thermally-activated polymerization. The effect of shrinkage due to the polymerization is not appreciates in the dilatometry analysis, nevertheless both effects are present during the debinding if the green body is not totally polymerized. Moreover, before the exothermic peak, degradation of the uncured and cured resin causes an expansion of the green body due to the escaping of the formed gases. Thus, both phenomena generate stresses on the green body which causes it to crack.

This crack formation was not observed for the 25 μm pieces, which could be explained by the less variation on the polymerization degree along the printed pieces, when compared with the 50 and 75 μm pieces. This result gives an indication that, perhaps, the samples with higher layer thickness may have more defects during the debinding process, since the polymerization degree is more critical.

5.4 Debinding process

5.4.1. Debinding in oxidative atmosphere

The initial experiments of the debinding process was performed in an oxidative atmosphere, air atmosphere concretely, once it is more convenient for both economic and technical point of view. Although the disadvantages of working in oxidative atmospheres are known, this study has the main goal of optimize the debinding factors to minimize or eradicate the defects generated during the thermal treatment.

As said, the relationship between cure depth and layer thickness is an important factor to avoid the delamination of the part. Following the reported results, the cure depth must be six times higher than the layer thickness. In this sense, the debinding study was performed on cylinders printed with 25 μm of layer thickness with 10 seconds of exposure time, which means a cure depth of 150 μm . The printed cylinders have a diameter of 10 mm, a high of 5 mm and a thickness of 2 mm. Theoretically, by optimizing the thermal treatment for a cylinder with 2 mm of thickness, pieces with lower thickness could be also successfully obtained. For higher thickness the thermal cycle must be re-adjusted.

The initial study of the debinding process has the main objective to analyze the effect of the temperature rate on the defect formation. In this study the debinding was performed until 500 $^{\circ}\text{C}$ at different temperature rates: 3, 0.5, 0.3 and 0.1 $^{\circ}\text{C}\cdot\text{min}^{-1}$, with a dwell time of 30 minutes. Figure 5.17 shows the cylinders after the debinding process performed at different rates. Note that a) is the printing plane and b) represents the z-direction, i.e., the building direction.

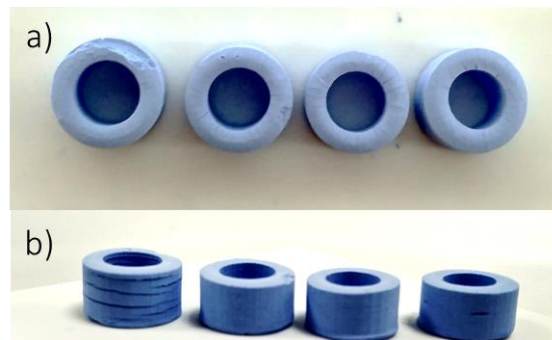


Figure 5.17 – Images of the a) top view and b) front view of the debinded cylinder at different temperature rates: 3, 0.5, 0.3 and to $0.1\text{ }^{\circ}\text{C}\cdot\text{min}^{-1}$ (from left to right).

As shown in the chapter IV the green pieces do not have any delamination or major defect between layers after the cleaning process. In this sense, the observed defects are directly related with the debinding process.

It is observed cracks on the top view of all samples. Moreover, the cylinder of $3\text{ }^{\circ}\text{C}\cdot\text{min}^{-1}$ presents a clear delamination. The formation of this defects becomes more evident as the debinding rate increases.

The X-Ray image technique was used for a deeper analysis of these defects. In fact, this is a powerful and non-destructive technique which give information about the whole sample and not just a superficial area. Figure 5.18 shows the same cylinders after the debinding process performed at different temperatures.

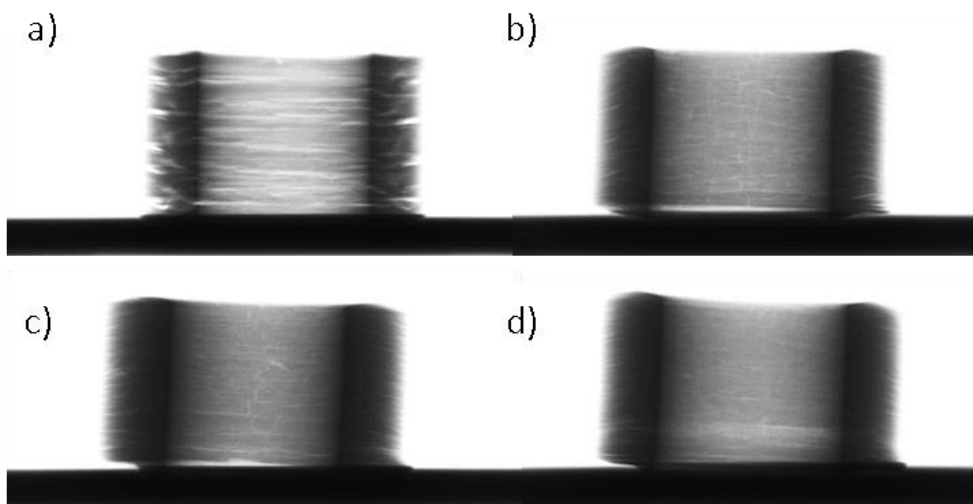


Figure 5.18 – X-ray image of debinded pieces at different rates a) $3\text{ }^{\circ}\text{C}\cdot\text{min}^{-1}$ b) $0.5\text{ }^{\circ}\text{C}\cdot\text{min}^{-1}$ c) $0.3\text{ }^{\circ}\text{C}\cdot\text{min}^{-1}$ and d) $0.1\text{ }^{\circ}\text{C}\cdot\text{min}^{-1}$ until $500\text{ }^{\circ}\text{C}$ in air atmosphere.

It is observed horizontal cracks in all samples, due to delamination between the layers, and also vertical cracks. However, the vertical cracks are not associated with the layer by layer fabrication. Thus, these defects could not be just associated to the building strategy, there are associated with the debinding process itself. Moreover, there are a clear relationship between temperature rate and crack formation, i.e, as the temperature rate increases the pieces present more cracks.

As said previously in the dilatometry study, by increasing the temperature rate the expansion of the pieces becomes more evident. This is associated to the highest rate of weight loss of the cured resin, which cause a huge amount of volatiles to escape out of the piece. At the same time the polymerization of uncured and/or less polymerized zones could also cause stress on the pieces.

In this regard, both weight loss by the decomposition of the resin and polymerization of non-cured region could cause internal stress and, consequently, the cracking of the green body. It was observed during the TGA analysis that reduction the temperature rates, the weight loss occurs at slower rate which could prevent the cracks formation. As shown in chapter IV, the printed parts present a 2-3 % of shrinkage after the printing process. Thus, the polymerization shrinkage during the printing process causes built-in stresses which can lead also to the deformation and delamination during the debinding process.

A cylinder piece printed with the same condition of the precious ones was heated until 200 °C at 0.3 °C·min⁻¹, to evaluate if the polymerization of the residual monomer and it weight loss before the exothermic peak could be related with the crack formation. Figure 5.19 shows the sample after the mentioned thermal treatment.

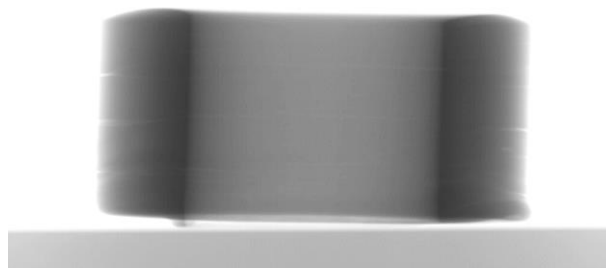


Figure 5.19 – X-ray image after the thermal treatment of 0.3 °C·min⁻¹ until 200 °C.

It appeared that the cracks formation began before the highest weight loss of the cured resin, and then became more severe during subsequent resin removal, as shown in Figure 5.18. Once the results shown in Figure 5.19 is before the significant weight loss due to degradation of the cured resin, the cracks formation at this temperature could be explained by the weight loss and polymerization of the residual monomer. Furthermore, to the release of the stresses previously induced during the printing process.

After the debinding process, a densification of the parts was achieved by the sintering process. This process was carried out up to 870 °C at 1 °C·min⁻¹, with a dwell time of 30 minutes. Figure 5.20 shows the x-ray images after the sintering process.

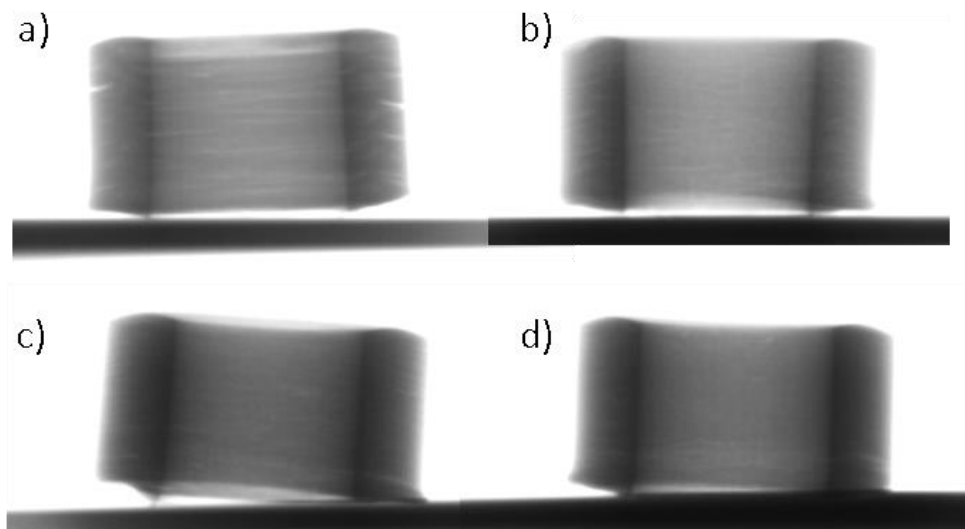


Figure 5.20 – X-ray image of sintered pieces, debinded at different rates a) 3 °C·min⁻¹ b) 0.5 °C·min⁻¹ c) 0.3 °C·min⁻¹ and d) 0.1 °C·min⁻¹.

It is observed that the sintering of the parts minimizes the delamination and cracks defects observed in the debinding. This can be explained by the liquid phase sintering, where the glass phase can act as a “soldering agent” minimizing these defects. Furthermore, the shrinkage itself during the sintering process also contribute to the final densification of the sintered parts.

Nevertheless, as observed in the x-ray images all samples still have defects. Figure 5.21 shows the SEM images of the front view of the sintered cylinders

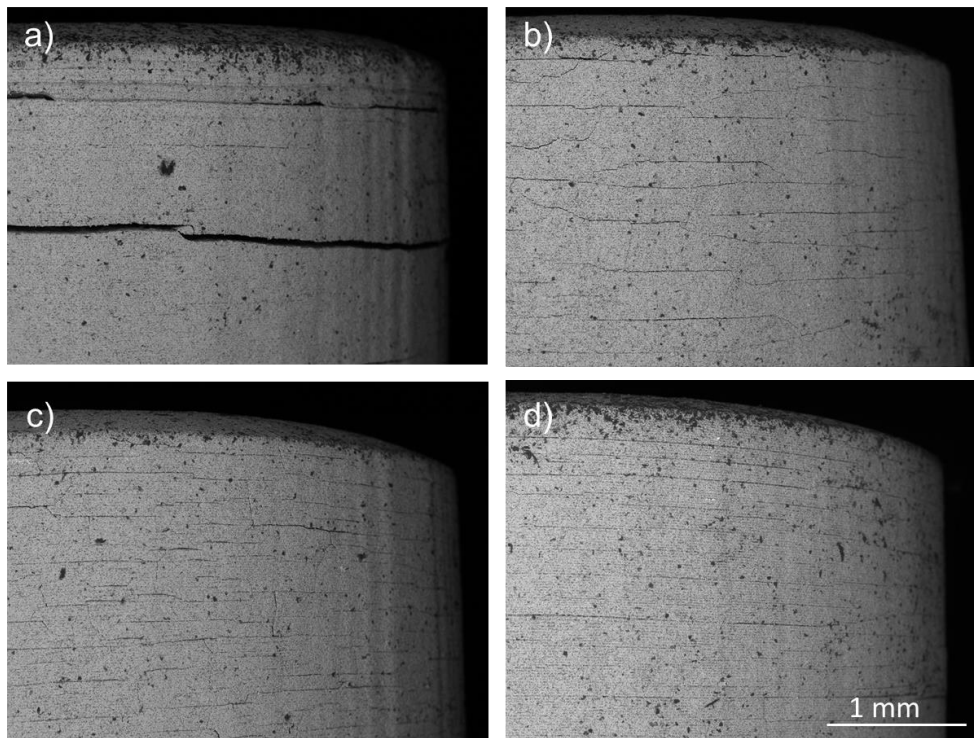


Figure 5.21 – SEM image of the sintered pieces, debinded at different rates a) $3\text{ }^{\circ}\text{C}\cdot\text{min}^{-1}$ b) $0.5\text{ }^{\circ}\text{C}\cdot\text{min}^{-1}$ c) $0.3\text{ }^{\circ}\text{C}\cdot\text{min}^{-1}$ and d) $0.1\text{ }^{\circ}\text{C}\cdot\text{min}^{-1}$ until $500\text{ }^{\circ}\text{C}$

It is observed that for the samples with the rate of $3\text{ }^{\circ}\text{C}\cdot\text{min}^{-1}$ during the debinding presents higher cracks displacement. As the temperature rate decreases in the debinding process, the cracks formation is reduced as well as its size.

Thus, a free-crack piece was not successfully obtained for the 2 mm thickness cylinder. However, the most satisfactory results were obtained for the debinding performed at $0.1\text{ }^{\circ}\text{C}\cdot\text{min}^{-1}$ of temperature rate.

Table 5.3 shows the obtained densities in function of the debinding rate, all of them with the sample sintering treatment ($1\text{ }^{\circ}\text{C}\cdot\text{min}^{-1}$ until $870\text{ }^{\circ}\text{C}$ with a dwell time of 30 minutes). For the density calculation of the sintered pieces, the density of the powder was measured by the AccuPyc 1330 Pycnometer resulting in a density of $3.3846 \pm 0.0028\text{ g}\cdot\text{cm}^{-3}$.

Table 5.3 – Densities results of the sintered pieces depending of the debinding rates in air atmosphere. The relative density percentage is calculated based in the LTCC density.

Debinding rate (°C·min ⁻¹)	Density (g·cm ⁻³)	Relative density (%)
3.0	2.883	85.2
0.5	2.986	88.2
0.3	3.012	89.0
0.1	3.039	89.8

It is observed that the final density of the cylinders presents a correlation with the debinding rate. Decreasing the debinding rate, the obtained density increases. This result is expected once the density of cracks and its sizes decreases when slower temperature rates are applied during the debinding process.

As the pieces geometry also influence the debinding process, a study of wall thickness and geometry was performed. In this study quadrangular and cylindrical pieces with 2, 1.5, 1 and 0.5 mm of wall thickness were printed. The debinding process was performed at 0.1 °C·min⁻¹ of temperature rate, once it was the one which provides better results. Moreover, the same sintering process were applied for this study, i.e., 1 °C·min⁻¹ until 870 °C with a dwell time of 30 minutes. Figure 5.22 shows the sintered samples with different geometry and wall thickness.

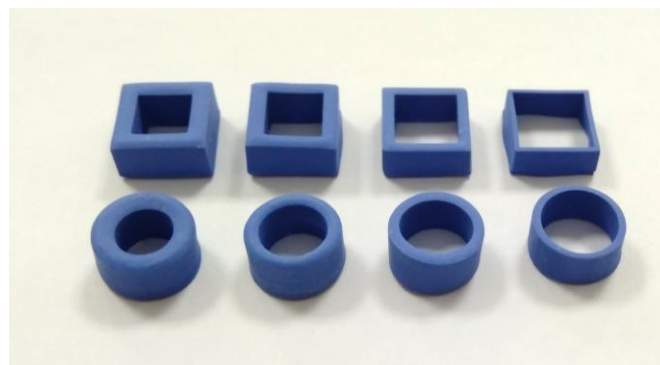


Figure 5.22 – Sintered pieces with different shape and wall thickness.

Figure 5.23 shows the SEM image of the quadrangular samples after the sintering process, printed with different wall thickness,

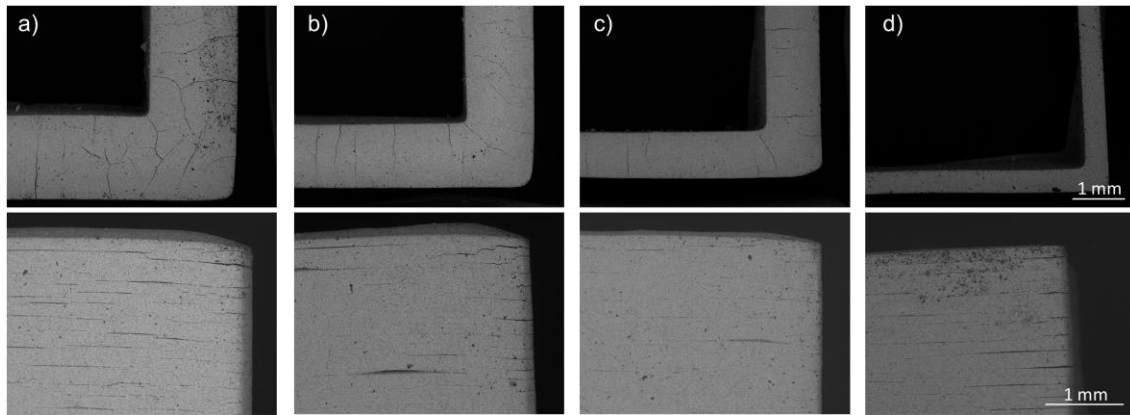


Figure 5.23 – SEM images of the sintered quadrangular pieces with different wall thickness: a) 2 mm b) 1.5 mm c) 1 mm and c) 0.5 mm. First row: top view and second row: front view.

It is observed that even with a wall thickness of 500 μm the cracks formation is unavoidable. However, the analysis of the top view of the samples shows that reducing the wall thickness the cracks do not appear in this plane, which corresponds to the XY-plane. In this sample the cracks appear just in the front view, related to the printing direction. Thus, it seems that the cracks formation has a preferential direction, which corresponds to the weaker zones, i.e., between layers.

The same study carried out for cylindrical samples, printed with different thicknesses. Figure 5.24 shows the SEM images of these cylinders, after the sintering process.

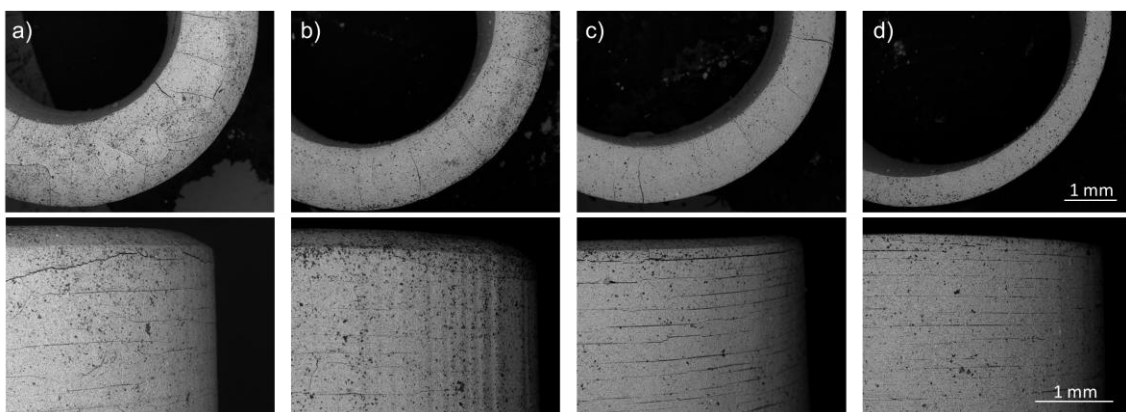


Figure 5.24 – SEM images of the sintered cylindrical pieces with different wall thickness: a) 2 mm b) 1.5 mm c) 1 mm and c) 0.5 mm. First row: top view and second row: front view.

All samples present cracks in both views, top and front, except for the samples with 500 μm , which does not present any major defect of the top view, as well as in the previous results. Moreover, it was not observed a clear difference between these results and the ones performed with the quadrangular samples. Thus, a correlation between sample geometry and cracks formation was not observed in this study.

By now, the results of the debinding and sintering process do not prevent the cracking of the printed pieces. In this regard, another debinding strategy was studied to improve these results. The following results are related to the use of a non-oxidative atmosphere for the pyrolysis of the organic compound.

5.4.2. Debinding in non-oxidative atmosphere

In this study, the debinding process was studied in absence of oxygen. In this sense, a non-oxidative gas was used during this process to create an oxygen free environment during the debinding process. The atmosphere used for this process was VARIGON H5 which is a two-component mixture containing 95 vol.% argon and 5 vol.% hydrogen (Ar/5%H₂).

The debinding study was performed using the same geometry as in the previous study, i.e., cylinders printed with 25 µm of layer thickness with 10 seconds of exposure time. The dimensions of the cylinders have a diameter of 10 mm, a high of 5 mm and a thickness of 2 mm.

As shown in the DSC and TGA analysis, the exothermic peak which is related to the polymerization of uncured resin decreases drastically its intensity if a non-oxidative atmosphere and slow temperature rates is applied. Moreover, the energy release during the polymerization process also decreases.

As seen previously in the oxidative debinding study, the cracking of the pieces was detected at 200 °C using a 0.3 °C·min⁻¹ temperature rate, Figure 5.19. Once, the degradation of the cured resin started after 200 °C, the cracks presented in this part can be associated with the degradation of the residual monomer presented in the printed part.

The same experiment presented in Figure 5.19 was performed, however under the Ar/5%H₂ atmosphere. Figure 5.25 shows the cylinder printed with 25 µm after the thermal treatment carried out at a temperature rate of 0.3 °C·min⁻¹ until 200 °C.



Figure 5.25 – X-ray image after the thermal treatment of $0.3\text{ }^{\circ}\text{C}\cdot\text{min}^{-1}$ until $200\text{ }^{\circ}\text{C}$ under $\text{Ar}/5\%\text{H}_2$ atmosphere.

It is observed that, contrary to the observed previously, the sample does not present any detectable crack. Thus, until this temperature the debinding process could be improved using a non-oxidative atmosphere.

In the DSC and TGA study, the weight loss associated to the degradation of the residual monomer presents the same behavior for both, air and N_2 experiments. In this regard, the factor which is different between both experiments is the intensity of the exothermic peak and the energy release. As observed in the DSC and TGA analysis, both factors intensity and energy release of the exothermic peak, decrease when a N_2 atmosphere were used and slow temperature rates was applied. Thus, the cracks formation is not related with the weight loss before the exothermic event but to the exothermic event itself.

In this session, the debinding process was studied at different temperature rate using a non-oxidative atmosphere. Figure 5.26 shows the x-ray images of the cylinders debinded at different temperature rate: 0.1, 0.3, 0.5 and $^{\circ}\text{C}\cdot\text{min}^{-1}$ until $500\text{ }^{\circ}\text{C}$, with a dwell of 30 minutes, under $\text{Ar}/5\%\text{H}_2$ atmosphere.

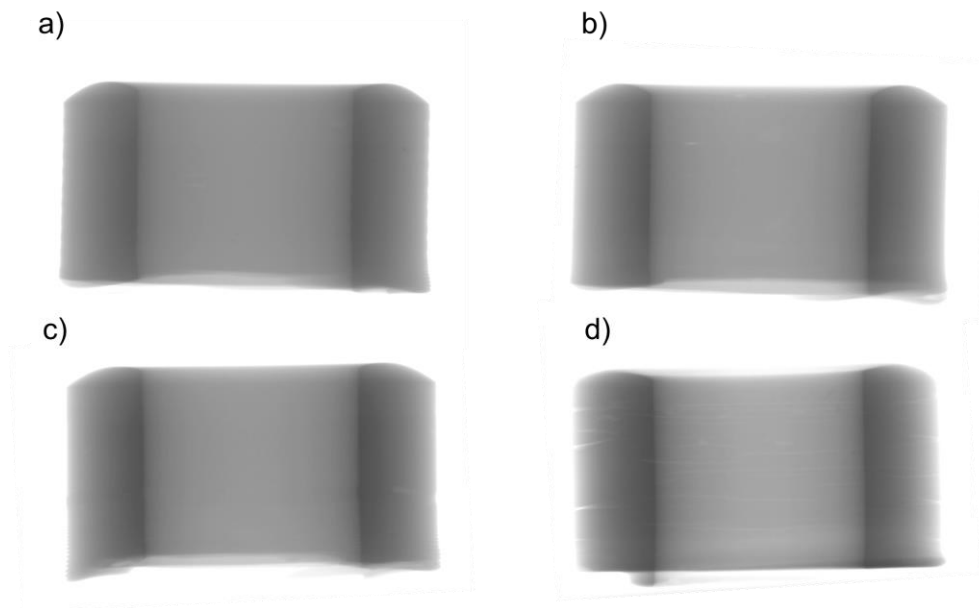


Figure 5.26 – X-ray image of debinded pieces at different rates a) $0.1\text{ }^{\circ}\text{C}\cdot\text{min}^{-1}$ b) $0.3\text{ }^{\circ}\text{C}\cdot\text{min}^{-1}$ c) $0.5\text{ }^{\circ}\text{C}\cdot\text{min}^{-1}$ and d) $1\text{ }^{\circ}\text{C}\cdot\text{min}^{-1}$ until $500\text{ }^{\circ}\text{C}$ in $\text{Ar}/5\%\text{H}_2$ atmosphere.

It is observed that the samples debinded at slower temperature rates ($0.1, 0.3$ and $0.5\text{ }^{\circ}\text{C}\cdot\text{min}^{-1}$) do not present any major defects. Nevertheless, for higher debinding rates ($1\text{ }^{\circ}\text{C}\cdot\text{min}^{-1}$) the horizontal cracks can be observed. This result can be explained by the increase of the exothermic peak intensity and the amount of energy release during the polymerization of the residual monomer. Moreover, the crack formation from the stresses produced during the printing process, due to the polymerization of the resin, could be also minimized reducing the temperature rate. The cracks are the consequence of the stress relaxation, in this sense for lower temperature rates this relaxation is performed in a progressive manner and do not cause a crack formation. On the other hand, if the temperature rate is too high, this relaxation occurs by a crack formation.

The 2 mm wall thickness cylinder was successfully obtained using a debinding rate until $0.5\text{ }^{\circ}\text{C}\cdot\text{min}^{-1}$, by using the non-oxidative atmosphere, preventing the cracking of the printed pieces. In this regard, there are a clearly improvement of the obtained resulting by changing the atmosphere during the debinding process. Nevertheless, a carbon residue is formed during this process due to the absence of oxygen for its combustion. This residue could be eliminated by using and oxidizing atmosphere.

As the sintering process is performed in air conditions, the elimination of these carbon residues can be complete in the sample thermal treatment.

A thermal treatment until 500 °C using the Ar/5%H₂ atmosphere was applied to a cured resin sample. After the thermal treatment the carbon residue was obtained, as a result of the pyrolysis process, which is the equivalent to the carbon residue presented in the debinded pieces of LTCC.

This carbon residue was analyzed by TGA measurement in air atmosphere, to study its decomposition behavior. Figure 5.27 shows the TGA at 10 °C·min⁻¹ in air atmosphere of the carbon residue.

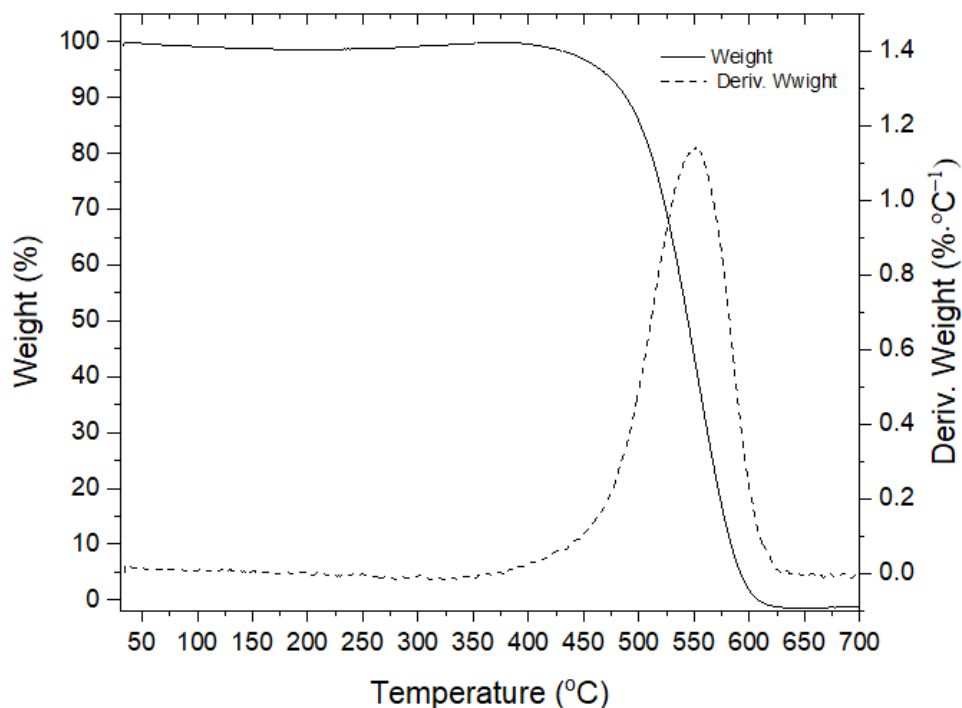


Figure 5.27 – TGA of the carbon residue at 10 °C·min⁻¹ in air atmosphere

It is observed the completed elimination of these carbon residue at 625 °C. This TGA was performed at 10 °C·min⁻¹, however it is known that if the temperature rate decreases this reaction occurs at lower temperatures. The elimination of this residue was performed during the sintering process, adding a step at 500 °C.

Thus, after the debinding process the pieces were submitted to the sintering where the residual char reacts with the oxygen, turning into carbon dioxide and water, before the densifications of the LTCC particles. As a result, a pure and dense ceramic piece could be obtained.

The sintering process was performed at $1\text{ }^{\circ}\text{C}\cdot\text{min}^{-1}$ until $870\text{ }^{\circ}\text{C}$ with a dwell of 30 minutes, an additional step was added to this process at $500\text{ }^{\circ}\text{C}$ with a dwell of 30 minutes for the carbon residue elimination. Figure 5.28 shows the x-ray results after the sintering process.

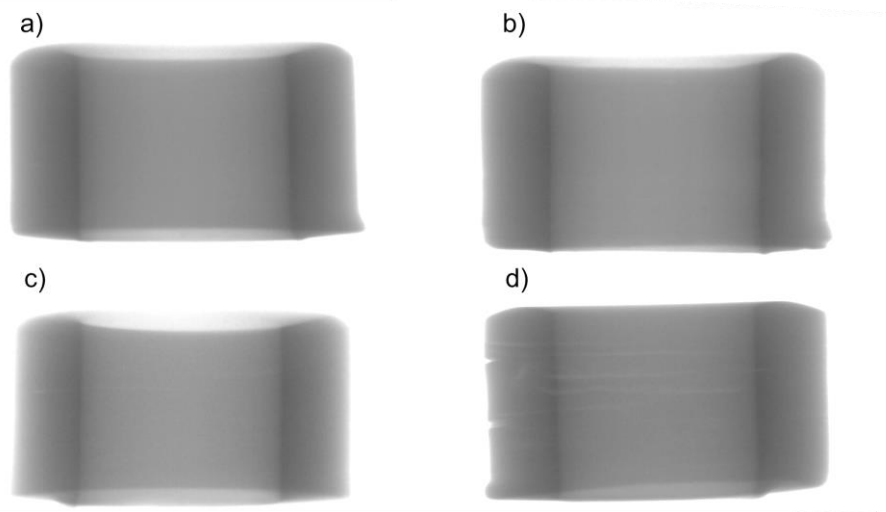


Figure 5.28 – X-ray image of sintered pieces at $870\text{ }^{\circ}\text{C}$, debinded at different rates a) $0.1\text{ }^{\circ}\text{C}\cdot\text{min}^{-1}$ b) $0.3\text{ }^{\circ}\text{C}\cdot\text{min}^{-1}$ c) $0.5\text{ }^{\circ}\text{C}\cdot\text{min}^{-1}$ and d) $1\text{ }^{\circ}\text{C}\cdot\text{min}^{-1}$ until $500\text{ }^{\circ}\text{C}$ in $\text{Ar}/5\%\text{H}_2$ atmosphere.

It is observed that the samples which did not present defect in the debinding process, i.e., the samples debinded at $0.1, 0.3$ and $0.5\text{ }^{\circ}\text{C}\cdot\text{min}^{-1}$, do not present any detectable defect. However, the samples which presented some defect on the debinding process ($1\text{ }^{\circ}\text{C}\cdot\text{min}^{-1}$) presents also some delamination after the sintering process. In fact, if the debinding process is successfully obtained, the sintering process do not represent a barrier to obtain a free-crack ceramic pieces, using a with a $1\text{ }^{\circ}\text{C}\cdot\text{min}^{-1}$ rate. Figure 5.29 shows the SEM images of the front view of the sintered cylinders.

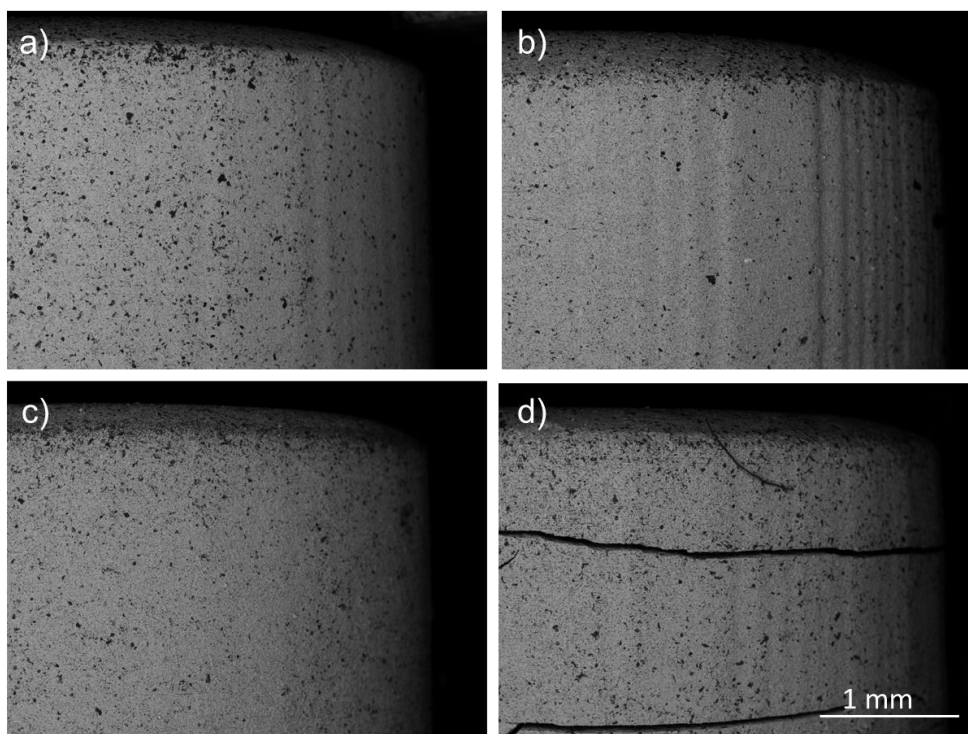


Figure 5.29 - SEM image of the sintered pieces, debinded at different rates a) $0.1\text{ }^{\circ}\text{C}\cdot\text{min}^{-1}$ b) $0.3\text{ }^{\circ}\text{C}\cdot\text{min}^{-1}$ c) $0.5\text{ }^{\circ}\text{C}\cdot\text{min}^{-1}$ and d) $1\text{ }^{\circ}\text{C}\cdot\text{min}^{-1}$ until $500\text{ }^{\circ}\text{C}$ in $\text{Ar}/5\%\text{H}_2$ atmosphere.

It can be observed a flat surface in the three cases of lower temperature rate during the debinding process. However, the one performed at $1\text{ }^{\circ}\text{C}\cdot\text{min}^{-1}$ presents large cracks. Thus, even doing the debinding process under absence of oxygen, the temperature rate cannot exceed $0.5\text{ }^{\circ}\text{C}\cdot\text{min}^{-1}$ to avoid the crack formation.

Table 5.4 shows the obtained densities in function of the debinding rate in $\text{Ar}/5\%\text{H}_2$ atmosphere, all of them with the sample sintering treatment ($1\text{ }^{\circ}\text{C}\cdot\text{min}^{-1}$ until $870\text{ }^{\circ}\text{C}$ with a dwell time of 30 minutes and the additional step of carbon residue removal).

Table 5.4 – Densities results of the sintered pieces depending of the debinding rates in $\text{Ar}/5\%\text{H}_2$ atmosphere. The relative density percentage is calculated based in the LTCC density.

Debinding rate ($^{\circ}\text{C}\cdot\text{min}^{-1}$)	Density ($\text{g}\cdot\text{cm}^{-3}$)	Relative density (%)
1.0	3.094	91.4
0.5	3.213	94.9
0.3	3.205	94.7
0.1	3.232	95.5

It can be observed that the samples with a debinding rate lower than $0.5\text{ }^{\circ}\text{C}\cdot\text{min}^{-1}$ presents similar density values. These samples present represents the highest density obtained in this work, with a density of 95 %.

In this sense, the optimal debinding is at $0.5\text{ }^{\circ}\text{C}\cdot\text{min}^{-1}$ of temperature rate under non-oxidative atmosphere for the maximum of 2 mm of wall thickness of the green body. The optimized thermal treatment, debinding and sintering, is presented in Figure 5.30.

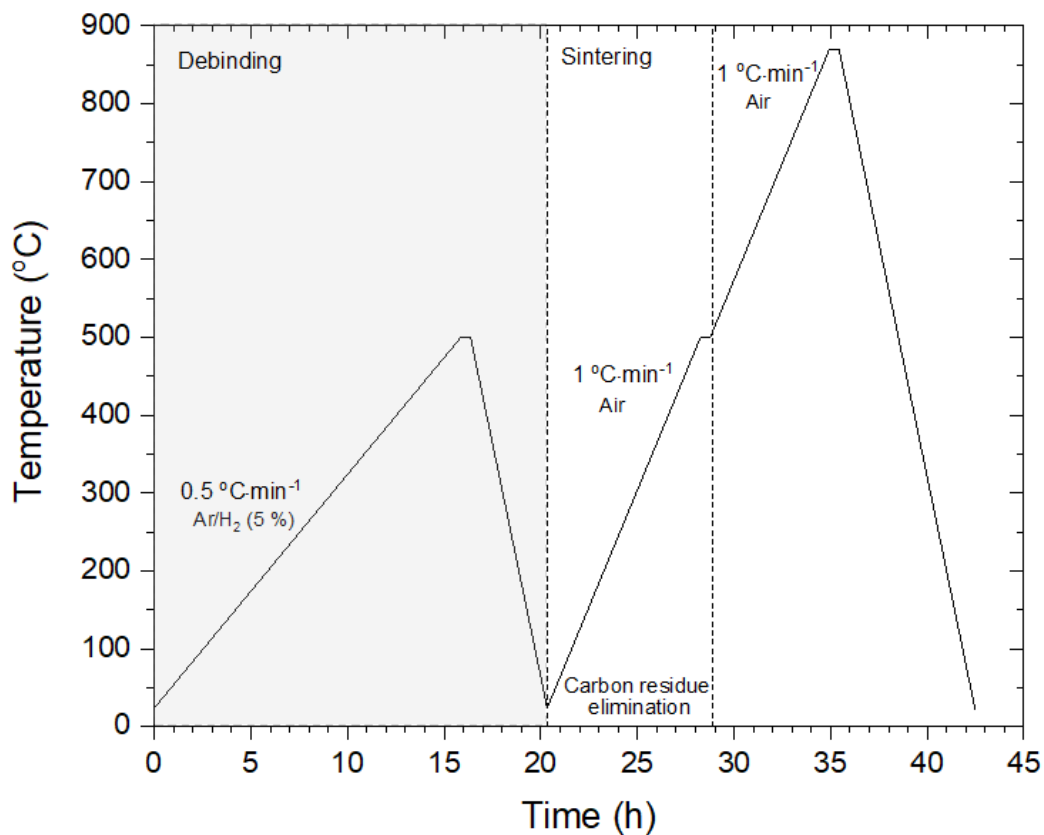


Figure 5.30 – Debinding and sintering thermal cycle.

The grey zone represents the debinding process, using a constant flow of Ar/5%H₂ during 20 h. The sintering process is presented in the white zone, where the carbon residue is also eliminated. The whole process takes 42 h, which means two days to obtain the final ceramic part.

The following results are related to influence of the layer thickness used for the printing on the debinding process results. Different cylinder with 2 mm of wall thickness, a diameter of 10 mm and a high of 5 mm were printed with different layer thickness: 25, 50 and 75 μm . In all cases, the cured of each layer were obtained by an exposure time of 10 seconds, which means a cure depth of 150 μm . In this sense, the relationship of layer thickness and cure depth is the variable in this study. The cure depth is six times higher than the layer thickness in the case of 25 μm of layer thickness and three and two times higher for the 50 and 75 μm of layer thickness ones.

The optimized debinding and sintering processes were used in this study. Note that the samples with 25 μm of layer thickness represents a repletion of the previous study.

Figure 5.31 shows the x-ray images of the three samples printed with different condition, i.e., different layer thickness with the same energy dose, after the debinding process.

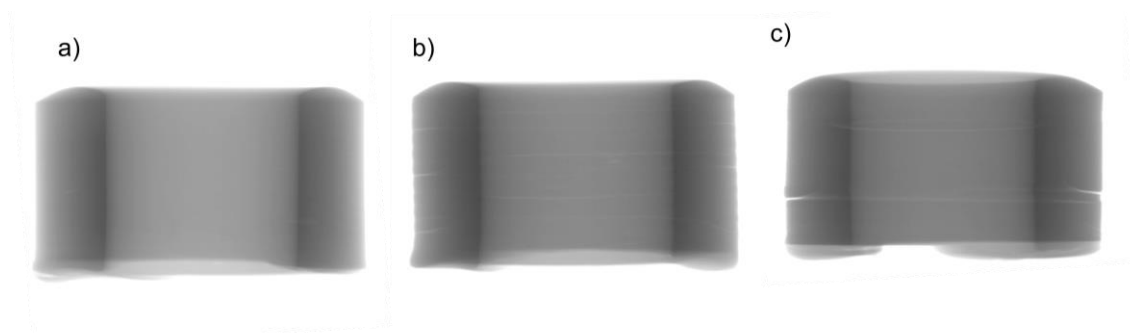


Figure 5.31 – X-ray image of debinded pieces printed with different layer thickness a) 25 μm b) 50 μm and c) 75 μm at 0.5 $^{\circ}\text{C}\cdot\text{min}^{-1}$ until 500 $^{\circ}\text{C}$ in Ar/5% H_2 atmosphere.

The x-ray results shows that the samples with 50 and 75 μm of layer thickness presents some delamination, however vertical cracks are not observed. As expected from the previous study, the sample which shows better results is the one printed with 25 μm with no delamination. As seen in the dilatometry results, the samples printed with 50 and 75 μm of layer thickness were the ones where the cracking were detected during the measurement. These results suggest that, by reducing the layer thickness the degree of polymerization is more homogeneous along the printed part, improving the debinding process. In fact, the used debinding rate were optimized for the samples printed with 25 μm of layer thickness. Thus, on hypothesis to successfully debinded the other samples is to reduce the

temperature rate. Figure 5.32 shows the x-ray results after the sintering process performed at $1\text{ }^{\circ}\text{C}\cdot\text{min}^{-1}$ until $870\text{ }^{\circ}\text{C}$, with the step at $500\text{ }^{\circ}\text{C}$ for the carbon residue elimination.

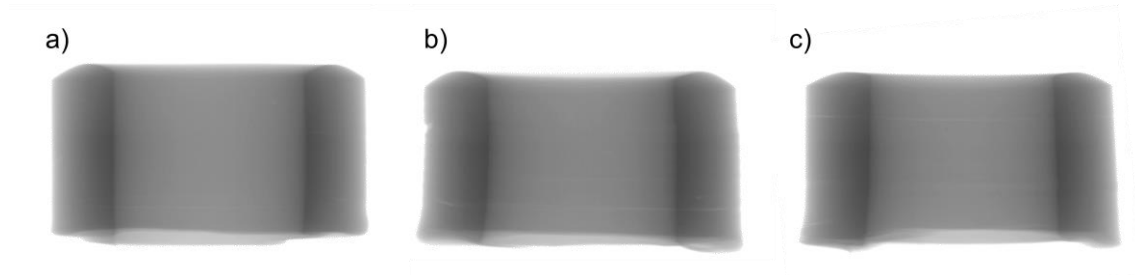


Figure 5.32 – X-ray image of the sintered pieces, printed with different layer thickness a) $25\text{ }\mu\text{m}$ b) $50\text{ }\mu\text{m}$ and c) $75\text{ }\mu\text{m}$ at $1\text{ }^{\circ}\text{C}\cdot\text{min}^{-1}$ until $870\text{ }^{\circ}\text{C}$ in air atmosphere.

The delamination presented in the debinding process in the samples printed with 50 and $75\text{ }\mu\text{m}$ of layer thickness is reduced. Fine cracks are observed in this samples, which are explained by the shrinkage during the sintering process and also due to the liquid phase sintering mechanism, as explained previously.

Figure 5.33 shows one of the cracks presented in the samples printed with $75\text{ }\mu\text{m}$ of layer thickness, after the sintered process. This image shows that, in fact, the glass phase can act as a “soldering agent” minimizing the cracking defects.

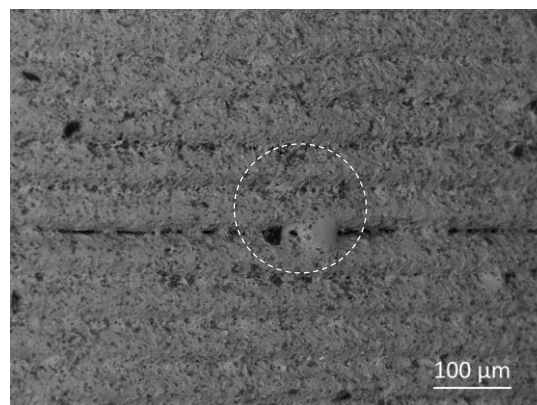


Figure 5.33 – SEM image of the sintered cylinder printed at $75\text{ }\mu\text{m}$ of layer thickness.

Table 5.5 shows the average shrinkage of the sintered samples with different layer thickness and its densities.

Table 5.5 – Densities and shrinkages results of the sintered printed with different layer thicknes. The relative density percentage is calculated based in the LTCC density.

Debinding rate (°C·min ⁻¹)	Shrinkage (%)		Density (g·cm ⁻³)	Relative density (%)
	z-direction	XY-plane ⁽¹⁾		
25	28.7	26.1	3.213	94.9
50	30.0	24.3	3.182	94.0
75	29.2	25.3	3.169	93.6

⁽¹⁾ – External diameter of the cylinder.

The shrinkage is similar in all cases, around 29 % in the z-direction and 25 % in the XY-plane. Thus, the shrinkage presents a higher value along the z-direction, i.e., the printing direction, than in the XY-plane which represents the projected area. A correlation of shrinkage and layer thickness was not observed in this experiment. The obtained densities are really similar between them, however the samples with 25 µm presents the highest value.

In this sense, the printing parameter could be a 25 µm to allow the debinding process at 0.5 °C·min⁻¹. Figure 5.34 shows the cylinder with 2 mm of wall thickness and printed with 25 µm of layer thickness. This figure shows the green body, after the printing and cleaning process, the debinded cylinder, after the pyrolysis process and finally, the sintered part.

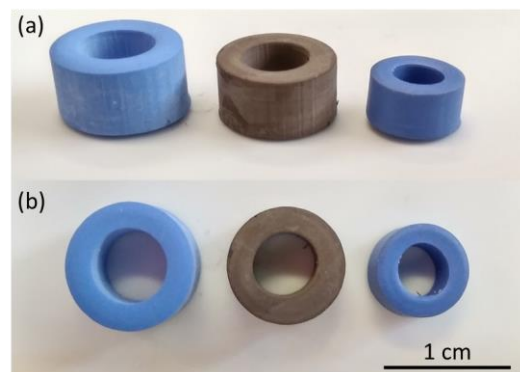


Figure 5.34 – Image of a) front view and b) top view of cylinders printed with 25 µm of layer thickness at different phases of the thermal treatment. On the left is the green body, in the middle the debinded and on the right the sintered one.

Figure 5.35 shows the SEM images of the sintered part, where the top and front view can be observed. Moreover, the microstructure is also presented in this figure.

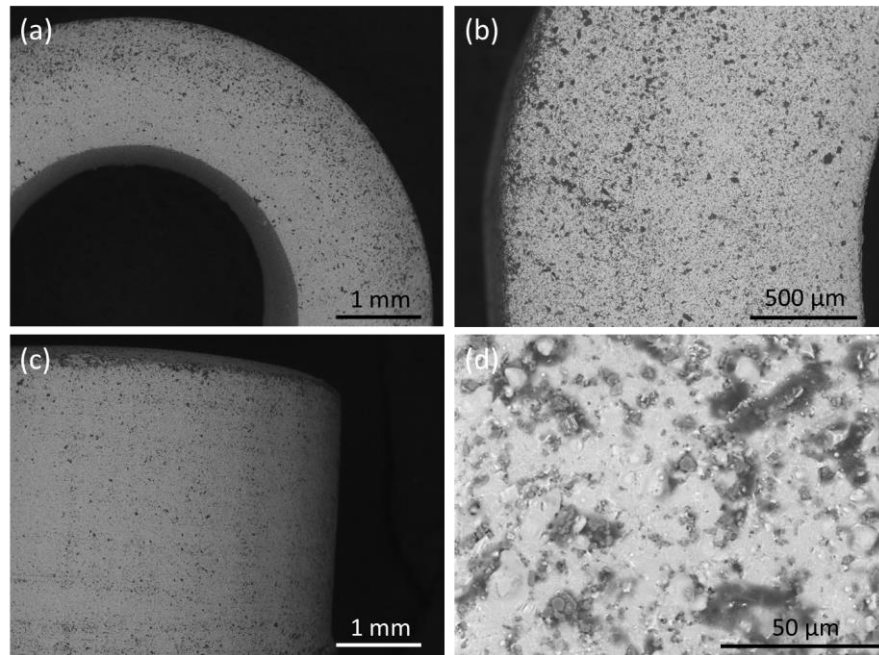


Figure 5.35 – SEM image of a) and b) top view and b) front view of sintered cylinders. d) the microstructure of the sintered cylinder.

A free-crack surface in both views is observed. In the microstructure image, both phases can be observed. The white one corresponds to the glass phase and the darker one to the crystalline phase of alumina.

These samples are deeper analyzed in terms of mechanical properties along the z-direction and phases identification.

Nanoindentation tests were performed on a Nanoindenter XP equipped with a continuous stiffness measurements (CSM) modulus and Berkovich tip indenter. In order to achieve statistical signification, a high number of indentations were performed: 576 (360 x 360 square), spaced 15 μm at 2000 nm of maximum penetration depth. The values of elastic modulus or Young' modulus (E) were calculated with the Oliver and Pharr method given by the software. For this analysis, the sample was embedding in a resin and properly polished.

The CSM measure the E along the 2000 nm in depth, however the average of E was calculated at a penetration depth between 600 and 1800 nm for each indentation. The main objective of this study is to evaluate if the layer-by-layer printing style affect the mechanical property of the sintered part. Figure 5.36.a presents the sintered cylinder and the identification of the area where the indentation was performed (with an inclination of 20° to obtain information between layers). Figure 5.36.b shows the SEM image of the some indentations.

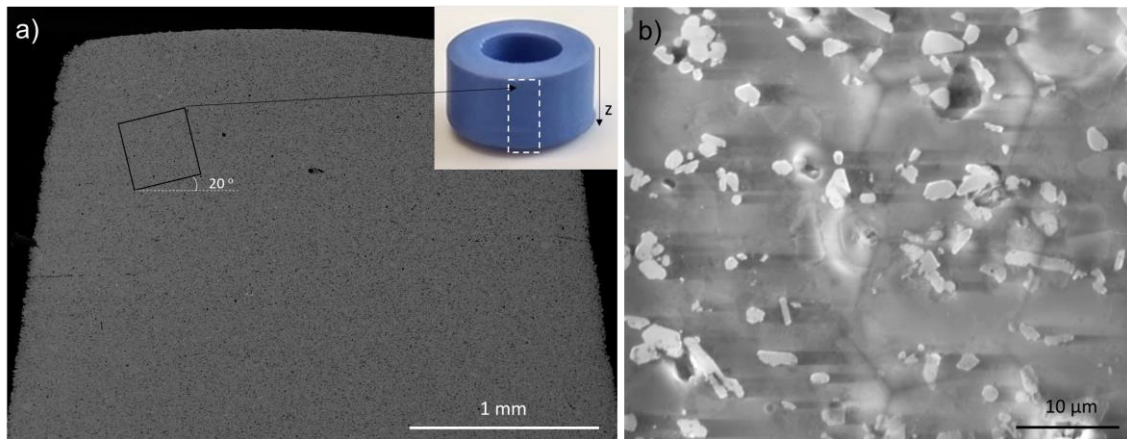


Figure 5.36 – a) SEM image of the polished surface in the z-direction with a scheme of the indentation area b) SEM image of indentation.

Figure 5.37 display the curves of the young' modulus vs. penetration depth for three different indentations, representing the highest E value, the average E value, and the minimum E value. The dashed lines represent the range of displacement into surface where the E average was performed of the all indentations.

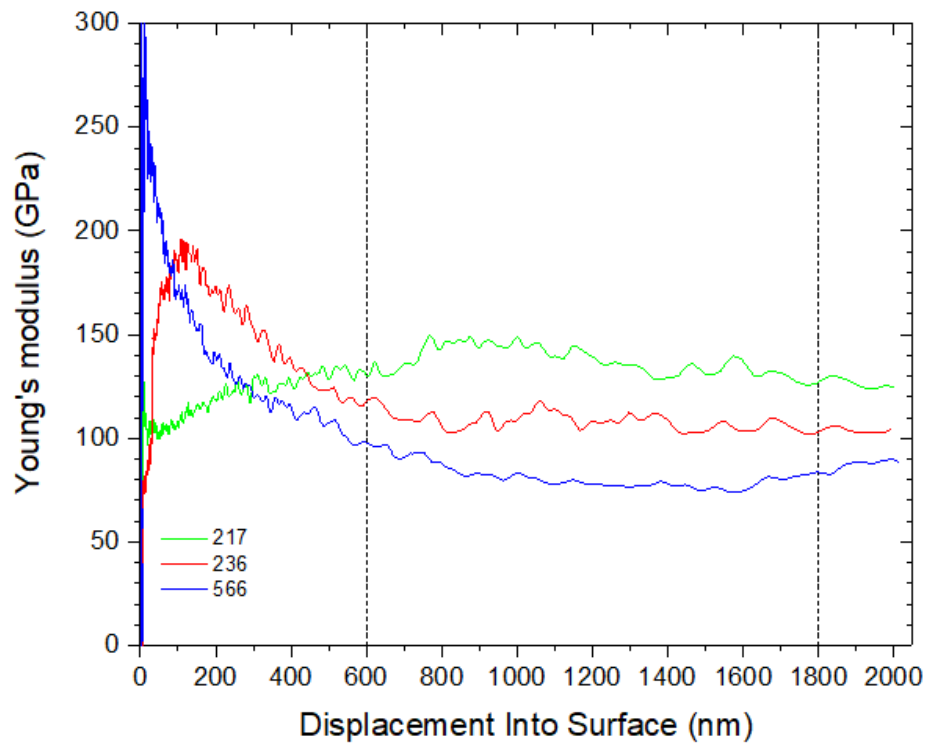


Figure 5.37 – Young's modulus vs. displacement into surface at different indentation

The mapping of the Young's modulus value for each indentation is presented in Figure 5.38 (along the $360 \times 360 \mu\text{m}^2$ area, separated $15 \mu\text{m}$ in both directions). The presented values are the average of E between 600 and 1800 nm of penetration depth.

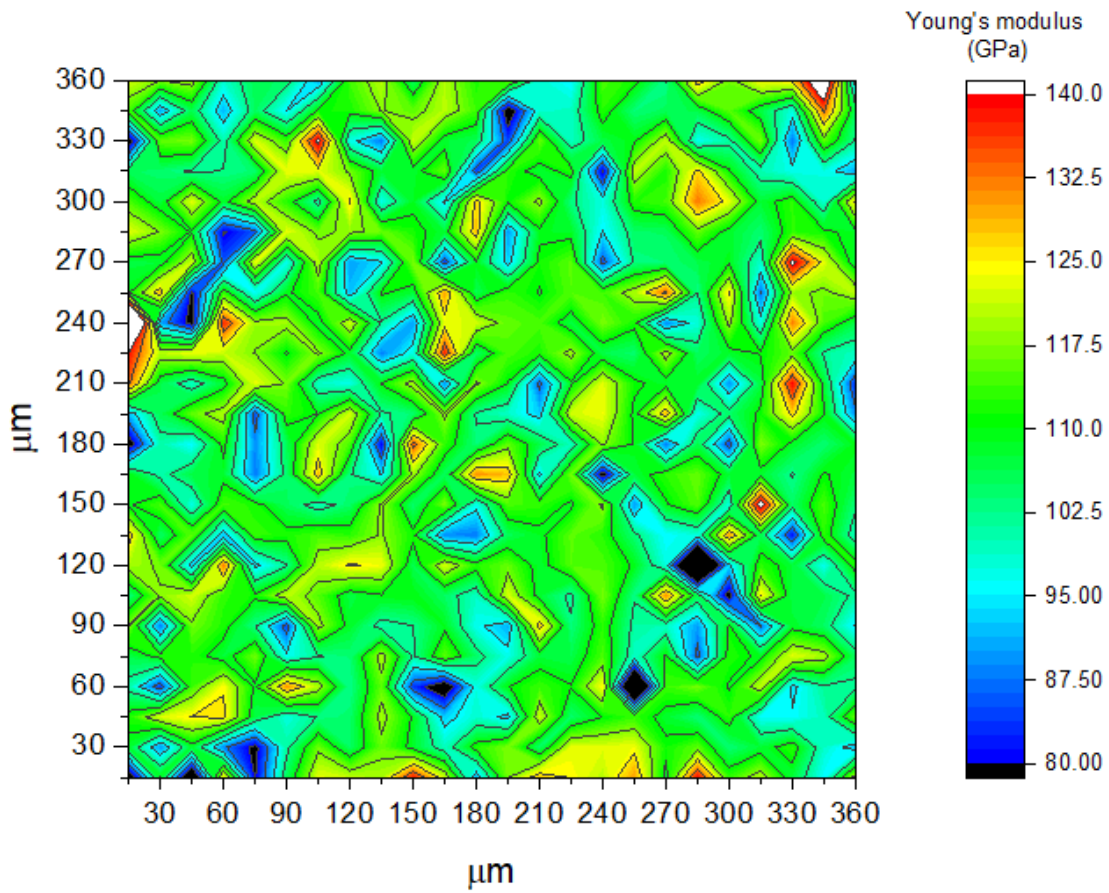


Figure 5.38 – Mapping of the average value of the young' modulus for the whole area (360 x 360 μm).

The printed piece shows an isotropic behavior in terms of mechanical properties, independent of the layer-by-layer strategy. The observed differences of the Young's modulus values are associated with the LTCC phases, resulting in E value around 140 GPa for the contribution of the hardest phases and around 80 GPa for the contribution of the softest phases. Moreover, the distribution of the Young's modulus values is uniformly distributed over the piece in concordance with the uniform distribution of the different phases of the LTCC.

The phases identification of the LTCC powder and after the sintering were analyzed by X-ray diffraction (XRD) technique.

X-ray diffraction (XRD) with Cu K_{α} radiation on a Brucker D8 Advance equipment was used to obtain information about the crystalline phases of the LTCC powder and the sintered pieces. The identification was performed by the X'Pert HighScore software database

The diffractogram of the LTCC powder is presented in Figure 5.39 with the corresponding peak identification. A SEM image is placed on the top right to show the morphology of the powder.

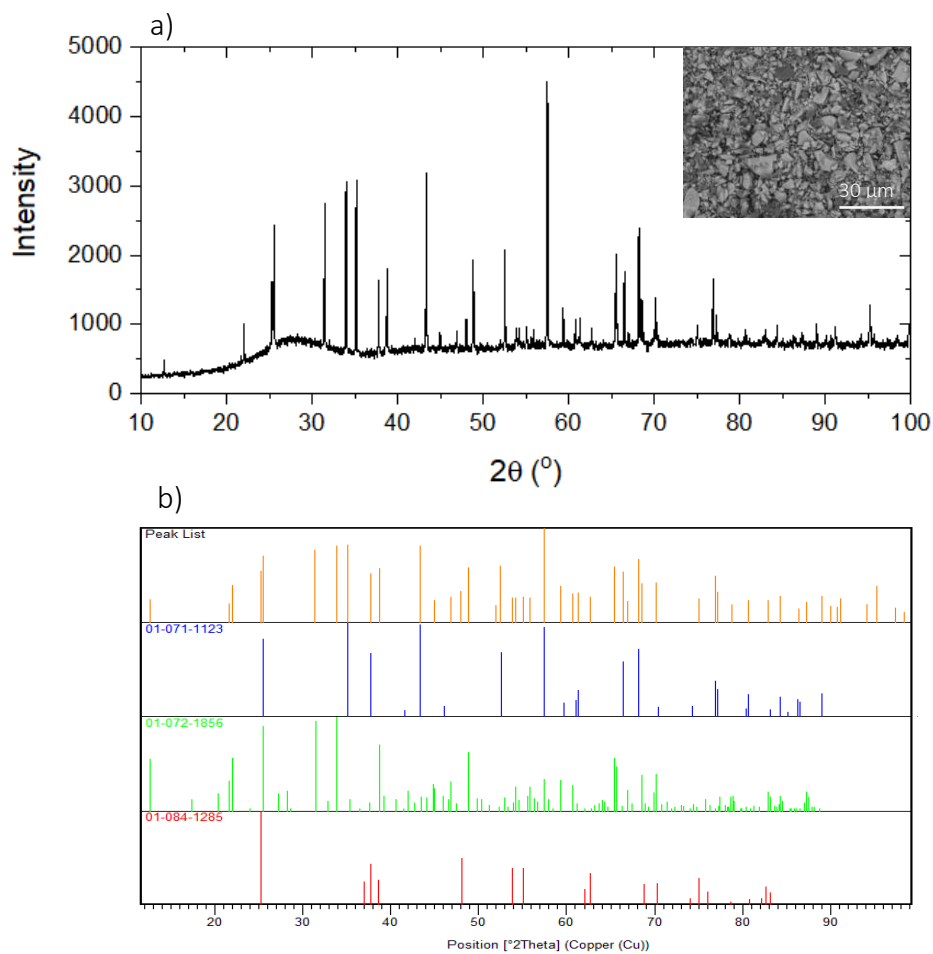


Figure 5.39 – a) XRD diffractogram of the LTCC powder with a SEM image on the top right and b) peak identification by X'Pert HighScore. Blue peaks: Corundum, Al_2O_3 . Green peaks: Willemite, Zn_2SiO_4 . Red peaks: Anatase, TiO_2 .

This analysis reveals that the main phase is the corundum (Al_2O_3), and it is also observed the presence willemite, Zn_2SiO_4 . The anatase (TiO_2) is also identified in the LTCC powder. In addition, it is evident the presence of the amorphous phase, between 20 and 35° due to the glass phase present in the LTCC powder.

Figure 5.40 display the diffractogram of the optimal sintered piece with the peak identification. The SEM image of the microstructure of the sintered LTCC piece.

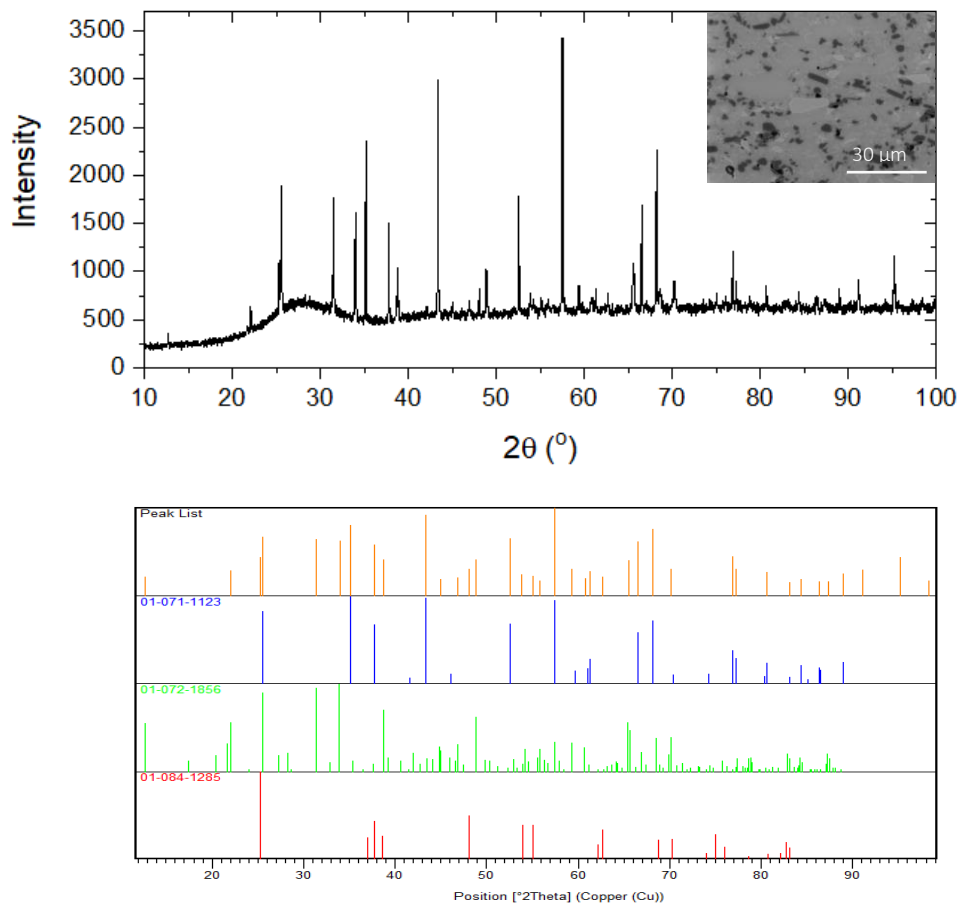


Figure 5.40 - a) XRD diffractogram of the LTCC sintered piece with a SEM image on the top right and b) peak identification by X'Pert HighScore. Blue peaks: Corundum, Al_2O_3 . Green peaks: Willemite, Zn_2SiO_4 . Red peaks: Anatase, TiO_2 .

This analysis shows that there are no new crystalline phases due to the sintering process, resulting in a same phase identification: corundum (Al_2O_3), willemite (Zn_2SiO_4) and anatase (TiO_2). The presence of the amorphous phase is also observed between 20 and 35° due to the glass phase present in the LTCC powder.

The phase identification in both raw LTCC powder and sintered LTCC piece are the same. Therefore, the optimized sintering process does not modify the compositions of the raw material.

5.5 Technology demonstrators

After the optimization of the whole process. i.e., the optimization of the LTCC suspension, the printing process and the thermal process, complex pieces could be successfully obtained. In this section, some examples of both LTCC pieces and multi-materials pieces are shown as a final result of the whole research and development presented in this work.

5.5.1. LTCC pieces

FAE company fabricates lambda sensors, which is an electronic device that measures the amount of oxygen in exhaust gases to adjust the air/fuel mixture. A part of the sensor itself, the whole device has other compounds for its assembling. Some of these components must be ceramic materials. In this regard, the re-design of these ceramic parts involves the fabrication of mold which has its associated cost and time-consumption. Thus, from a point of view of rapid prototyping these specific parts could be obtained directly from the CAD model, reducing the time and cost of the re-design process and reducing the time to market and the development cost. Moreover, not just the dimensional features can be evaluated, but also the final performance of these compounds once it could be printed directly with the functional material.

In this regard, Figure 5.41 shows some printed parts after the sintering process, used on the assembling of the lambda sensor, demonstrating the viability of the printing of this by MIP-SLA technology with the developed LTCC suspension.

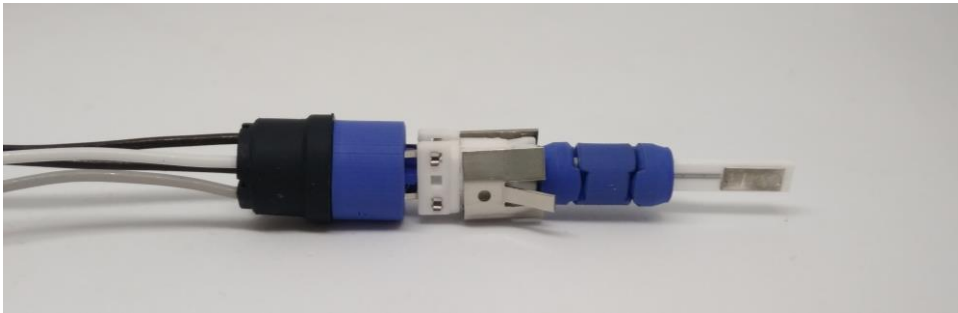


Figure 5.41 – Examples of the printed parts used for the redesign of the ceramic components of the lambda sensor.

Figure 5.42 shows the individual lambda sensor components printed by MIP-SLA using the developed LTCC suspension. It is also presented the original ceramic components, the white ones, in contrast with the LTCC printed ones (after the sintering process).

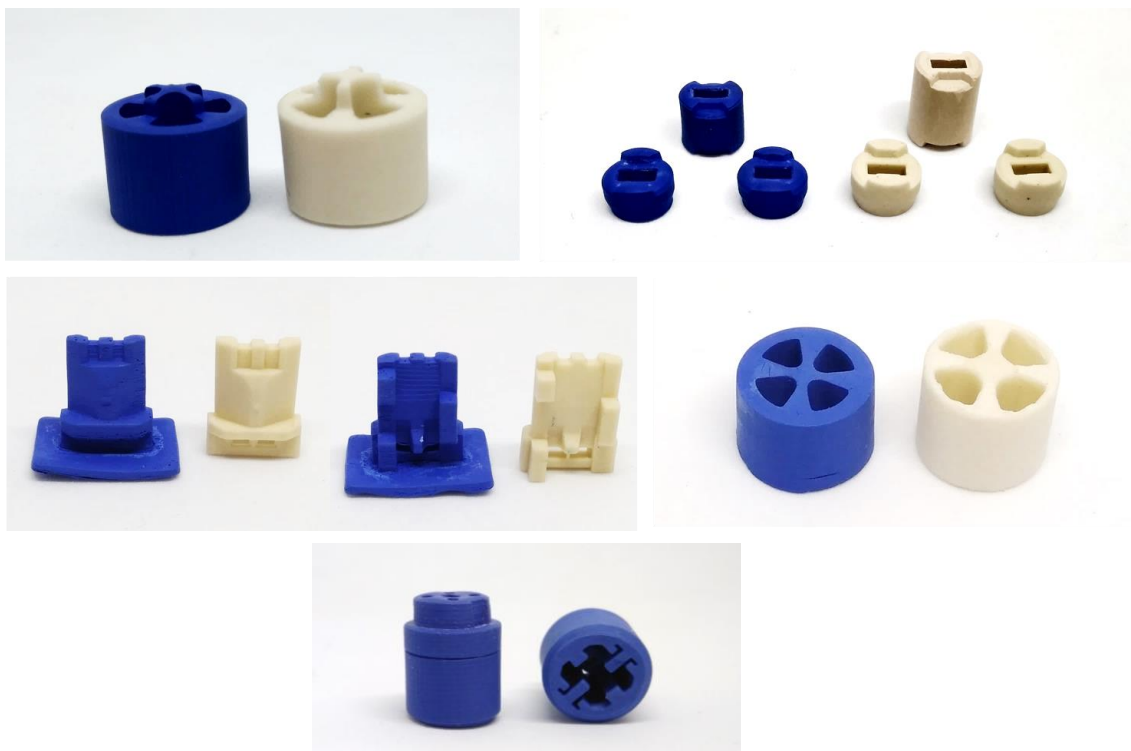


Figure 5.42 – Individual lambda sensor components printed by MIP-SLA technology (blue) ones and components fabricated by standard technology (white).

The ceramic materials used for this specific application are not a LTCC material, the one developed in this work. Nevertheless, the acquired knowledge in ceramic formulation for MIP-SLA technology and its debinding and sintering, could be applied on the development of other ceramic materials for this, or even for other applications. In this sense, the main objective of the shown pieces is to demonstrate that it can be fabricated by the developed technology, with high accuracy and directly with ceramic materials.

The following results have the main objective to demonstrate that ceramic parts with high accuracy and complexity could be obtained, using the developed LTCC suspension and MIP-SLA machine.

Figure 5.43 shows the green body and the sintered propeller-like geometry. This piece shows the ability to printing thin walls with a high level of torsion.

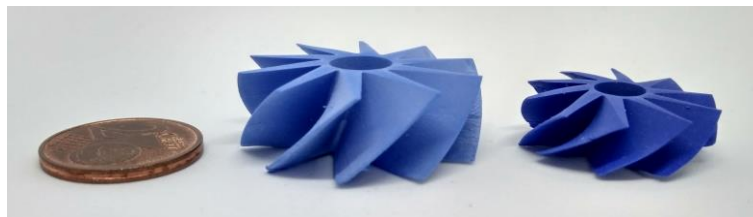


Figure 5.43 – Image of printed LTCC propeller a) green body and b) sintered part.

Figure 5.44 shows a ring after the printing and sintering processes. This piece shows the possibility of printing pieces with high level of detail/resolution for other applications, such as jewelry.



Figure 5.44 - Image of printed LTCC ring a) green body and b) sintered part.

5.5.2. Multi-material printing: a proof of concept

The final objective of this work is to demonstrate the proof of concept of the multi-material printing. During the sintering process, each material presents a specific behavior during the thermal treatment. The thermal shrinkage coefficient is associated for each material which also depend on the heat treatment applied.

As said previously, the MIP-SLA printer used in this work was developed under the NHIBIRD project. Moreover, the hybridization of the MIP-SLA and an inkjet printing system was also obtained in this project. Figure 5.45 shows the CAD model of the hybrid machine and the real image of this machine.

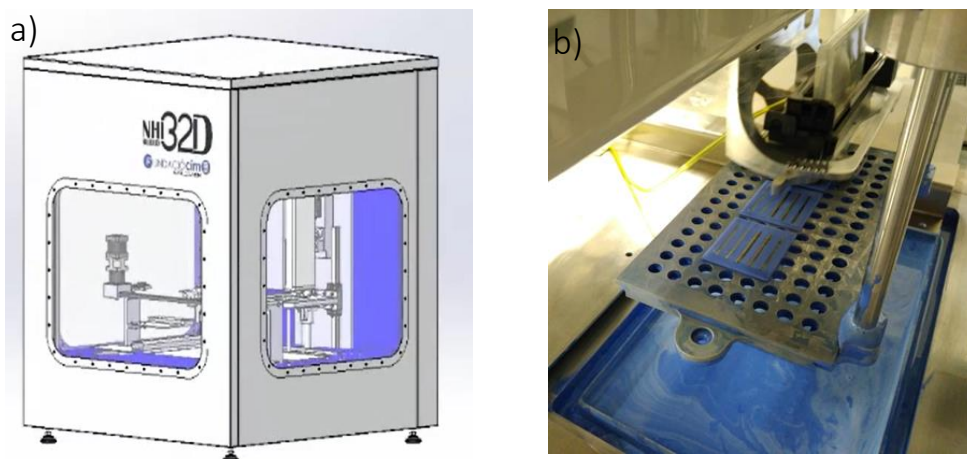


Figure 5.45 – Hybrid MIP-SLA and inkjet printing technology a) CAD model and b) real image.

An initial study of the co-sintering of silver nanoparticles with the LTCC is discussed in this section. The proof of concept of the multi-material printing is based on the printing of the LTCC substrate by MIP-SLA technology, and then, a conductive circuitry printed on it. This last process was performed using a Dimatix system, which is a piezo-based dispensing system. This system uses a cartridge with 21 μm of nozzle diameter. For a properly jetting of the silver particles, the particle size must be 100 times lower than the nozzle diameter. Thus, the 210 nm is the maximum for the particle size of the silver particles. Moreover, the

low viscosity is another restriction of this technology which do not allow the use of a high solid load ink.









A commercial silver ink was used for the printing of the conductive circuitry, from Advanced Nano Products Co., Ltd. The main characteristics of this ink is presented in Table 5.6.

Table 5.6 – Silver nanoparticle ink characteristics.

Characteristic	Value
Solid Content (wt.%)	30 - 35
Viscosity (mPa·s)	10 - 17
Curing Temp.(°C)	120-150
Specific Resistvity ($\mu\Omega\cdot\text{cm}$)	11-12

As expected, one of the principal issues of the hybridization of this technologies is the difference in terms of sintering temperature of the silver nanoparticles and the LTCC material. It must be considered that the layer thickness of the silver ink, deposited by the inkjet printing, is around 200-300 nm, which must be resist to the sintering process of the LTCC material. In this regard an optimization of number of numbers needed to remain after the sintering at 870 °C was studied, varying also the drop spacing (DS). This study was performed by the deposition of different layers, from 2 to 8 silver layers, with 50 and 35 μm of DS on a LTCC substrate. After the printing process the silver nanoparticles were sintered at 150 °C. Than the optimized thermal treatment, presented in Figure 5.30, was applied for the co-sintering process. Table 5.7 shows these results after the sintering process.

Table 5.7 – Study of DS and number of printed layers.

Drop spacing	Number of printed layers			
	2	4	6	8
50 μm				
37 μm				

It is observed that the silver ink does not remain after the sintering process in some. This is explained by the few amount of silver particles deposited during the inkjet printing. As the thermal treatment takes almost 2 days, reaching 870 °C, the silver nanoparticles tend to diffuse onto the LTCC structure. However, if the printing is performed a DS of 37 μm with 8 layers, the silver ink resists the thermal treatment.

Figure 5.46 shows another example of the multi-material printing using both technologies, displaying an image of the three different stages: after the printing process, after the debinding and finally, after the sintered process.

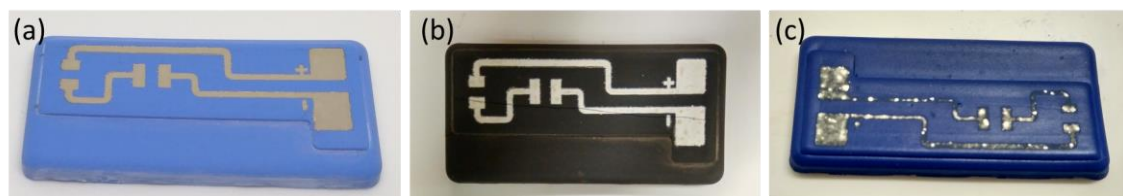


Figure 5.46 – Multimaterial piece: MIP-SLA and inkjet (6 layers) a) green body b) debinded and c) sintered.

It can be observed that after the debinding process, the silver circuitry remains with the same shape as the printed one. However, after the sintering process the silver material seems to be placed in specific points along the printed path. This can be explained by the melting of the silver during the sintering process. In some segments of the silver paths an electrical conductivity was observed. However, for the full conductivity of the circuitry the number of layers must be optimized.

The integrated inkjet system must work with nanoparticles at low solid load. This leads to a few particle depositions during the printing process. For many applications such as flexible printing, this technique provides high resolution and high conductive circuitry by sintering the nanoparticles at 120-150 °C. However, when the main goal is the co-sintering with ceramic materials, the amount of deposited silver particles is a critical point for the conductive patterns.

In this regard, the further optimization must be the focus of the number of layers, in the preparation of the LTCC surface for the inkjet printing, in the design of the circuitry and in the printing of embedded circuits on the LTCC material. Moreover, the hybridization of the MIP-SLA with different technologies is also a possibility to improve the results.

Conclusions

The studies summarized in this section provide conclusive evidence of the relevance of the temperature rate and atmosphere for a successful debinding of the ceramic green bodies.

The presence of oxygen in the debinding atmosphere negatively affects the process due to the polymerization of the residual monomer. As a result, the debinding process could not be successfully obtained in air atmosphere, even for samples with 500 μm of wall thickness and lowering the temperature rate at $0.1\text{ }^{\circ}\text{C}\cdot\text{min}^{-1}$.

The debinding process was analyzed and performed in two different atmospheres: oxidative and non-oxidative. The exothermic peaks related to the polymerization of the uncured monomer were observed in both atmospheres, however the energy peak intensity is higher for the experiments performed in the oxidative one. The exothermic peak in the oxidative atmosphere presents a higher specific enthalpy and higher intensities, because polymerization of and oxidation of some radical monomers occurs simultaneously, and both phenomena involve exothermic reactions.

The polymerization of the monomer is not uniform along the cured depth, and as a consequence, the degradation of the resin occurs differently along the green body. In this regard, thermal degradation proceeds uniformly when a non-oxidative atmosphere and slow temperature rates are applied during the debinding process. The exothermic peak, associated with the polymerization of the residual monomer, decreases in intensity due to the reduction in temperature rate and using a non-oxidative atmosphere. Moreover, the energy released is also minimized under this condition, preventing the formation of cracks during the debinding process.

The delamination for the debinded pieces also occurs when the process is performed under a non-oxidative atmosphere. However, this defect occurs for debinding rates higher than $0.5\text{ }^{\circ}\text{C}\cdot\text{min}^{-1}$.

In conclusion, the maximum debinding rate is $0.5\text{ }^{\circ}\text{C}\cdot\text{min}^{-1}$ in a non-oxidative atmosphere, for a certain geometry and printing conditions, i.e., for cylinders of 10 mm diameter, a height

of 5 mm and a wall thickness of 2 mm, printed with 25 μm of layer thickness with 10 seconds of exposure time, which means a cure depth of 150 μm . By increasing the layer thickness to 50 and 75 μm , using the same energy dose, some slight delamination was observed after the debinding process. In this regard, the relation between cure depth and layer thickness is optimal when the cure depth is six times higher than the layer thickness, preventing the cracking of the pieces during the thermal debinding.

During the debinding process under a non-oxidative atmosphere, the carbon residues from the thermal degradation are eliminated in a previous step of the sintering process, in an oxidative atmosphere. At the sintering step, a dwell at 500 $^{\circ}\text{C}$ is performed for its elimination, followed by the densification of the pieces at 870 $^{\circ}\text{C}$. It was demonstrated that if the pieces do not present defects after the debinding process, the sintering could be performed at a higher rate ensuring a correct densification, without cracking. The final density after the whole optimized thermal treatment is 3.213 $\text{g}\cdot\text{cm}^{-3}$, meaning 95 % with respect to the theoretical density.

Regarding the nanoindentation, it was demonstrated that the sintered piece shows an isotropic behavior in terms of mechanical properties, independent of the layer-by-layer strategy. The observed differences of the Young's modulus values are associated with the LTCC phases, resulting in E value around 140 GPa for the contribution of the hardest phases and around 80 GPa for the contribution of the softest phases. Moreover, the distribution of the Young's modulus values is uniformly distributed over the piece in concordance with the uniform distribution of the different phases of the LTCC.

The successfully fabrication of complex pieces validates the whole process: from the LTCC suspension to the final thermal treatment.

Moreover, the proof-of-concept of AM hybridization was demonstrated by a multimaterial printed piece, indicating that the number of silver layers printed by the inkjet system is critical for the debinding and sintering processes.

References

- [1] J. A. Lewis, "Direct Observation of Preceramic and Organic Binder Decomposition in 2-D Model Microstructures," *J. Am. Ceram. Soc.*, vol. 77, pp. 1839–1845, 1994.
- [2] T. Ring, "Binder Burnout," in *Fundamentals of Ceramic Powder Processing and Synthesis*, 1996, pp. 729–775.
- [3] J. A. Lewis, "Binder removal from ceramics," *Annu. Rev. Mater. Soc.*, vol. 27, pp. 147–173, 1997.
- [4] C. L. Beyler and M. M. Hirschler, "Thermal Decomposition of Polymers," in *Fire Protection Engineering*, 2016, pp. 1–131.
- [5] R. K. Enneti, S. J. Park, R. M. German, and S. V. Atre, "Review : Thermal Debinding Process in Particulate Materials Processing," *Mater. Manuf. Process.*, vol. 27, pp. 103–118, 2012.
- [6] C. Bae and J. W. Halloran, "Influence of Residual Monomer on Cracking in Ceramics Fabricated by Stereolithography," *Int. J. Appl. Ceram. Technol.*, vol. 8, pp. 1289–1295, 2011.
- [7] M. Trunec and J. Cihlg, "Thermal Debinding of Injection Moulded Ceramics," *J. Eur. Ceram. Soc.*, vol. 17, pp. 203–209, 1997.
- [8] M. Trunec and J. Cihlar, "Removal of thermoplastic binders from ceramic green bodies," *Ceramics*, vol. 41, pp. 67–80, 1997.
- [9] E. Johansson, O. Lidström, J. Johansson, O. Lyckfeldt, and E. Adolfsson, "Influence of Resin Composition on the Defect Formation in Alumina Manufactured by Stereolithography," *Materials (Basel)*, vol. 10, pp. 1–11, 2017.
- [10] G. Mitteramskogler *et al.*, "Light curing strategies for lithography-based additive manufacturing of customized ceramics," *Addit. Manuf.*, vol. 1–4, pp. 110–118, 2014.
- [11] P. Markus, M. Gerald, G. Robert, and S. Jürgen, "Thermal debinding of ceramic-filled photopolymers," *Mater. Sci. Forum*, vol. 825–6, pp. 75–81, 2015.
- [12] U. Scheithauer, E. Schwarzer, T. Moritz, and A. Michaelis, "Additive Manufacturing of Ceramic Heat Exchanger : Opportunities and Limits of the Lithography-Based Ceramic Manufacturing (LCM)," *J. Mater. Eng. Perform.*, vol. 27, pp. 14–20, 2018.

- [13] U. K. Fischer, N. Moszner, V. Rheinberger, W. Wachter, J. HOMA, and W. Längle, "Light-Curing Ceramic Slips for the Stereolithographic Preparation of High-Strength Ceramics," US20140183799A1, 2010.
- [14] C. Chapat, C. Thierry, and D. Franck, "Method and Composition for Making Ceramic Parts by Stereolithography and Use in Dentistry," US20050090575A1, 2005.
- [15] A. M. Knapp and J. W. Halloran, "Binder Removal from Ceramic-Filled Thermoplastic Blends," *J. Am. Ceram. Soc.*, vol. 89, pp. 2776–2781, 2006.
- [16] M. T. Sebastian and H. Jantunen, "Low loss dielectric materials for LTCC applications : a review," *Int. Mater. Rev.*, no. March, 2008.
- [17] Y. Imanaka, *Multilayered Low Temperature Cofired Ceramics (LTCC) Technology*. 2005.
- [18] V. V. Krongauz, "Crosslink density dependence of polymer degradation kinetics : Photocrosslinked acrylates," *Thermochim. Acta*, vol. 504, pp. 70–84, 2010.
- [19] P. J. Bártolo, *Stereolithography: Materials, Processes and Applications*. Springer, 2011.
- [20] A. Goswami, G. Srivastava, A. M. Umarji, and G. Madras, "Thermal degradation kinetics of poly (trimethylol propane triacrylate)/ poly (hexane diol diacrylate) interpenetrating polymer network," *Thermochim. Acta*, vol. 547, pp. 53–61, 2012.

